Rev.Adv.Mater.Sci. 6 (2004) 94-119

STRUCTURAL PROPERTIES OF DIAMOND NANOWIRES: THEORETICAL PREDICTIONS AND EXPERIMENTAL PROGRESS

Amanda S. Barnard

Center for Nanoscale Materials, Argonne National Laboratory, 9700 South Cass Ave, Argonne, IL, 60439, USA

Received: February 17, 2004

Abstract. Although the nanoscience and nanotechnology surrounding sp^2 bonded carbon nanotubes has continued to flourish over recent years the development of the sp^3 analogue, diamond nanowires, has been slow. Diamond-based materials have unique structural properties such as high elastic modulus and strength-to-weight ratio, making them ideal candidates for structural applications at the nanoscale. While few experimentalists have succeeded in synthesizing such materials, a number of researchers have used various theoretical models to compare the structure and stability of diamond nanowires as a function of morphology and size. In this review a summary of these theoretical predictions is given along with the progress made by experimentalists in the synthesis of quasi-one dimensional diamond nanostructures.

1. INTRODUCTION

With the variety of quasi-zero dimensional (0-D) carbon materials available to nanoscience and technology, it comes as no surprise that the attention of many nanotechnologists is focussed around carbon-based nanostructures [1,2]. Nano-size carbon particles such as fullerenes, carbon onions and nanodiamond represent the 0-D analogues of three-dimensional sp^2-bonded graphite and sp^3-bonded diamond. At a fundamental level, the study of nanocarbon continues to highlight that at the nanoscale such structures differ from their macroscopic counterparts, possessing unique properties due entirely to their finite size [2]. The existence of multiple nanocarbon phases does however raise the questions as to how they are related to one another, and as to which phase is energetically preferred in a given size regime. Therefore, a great deal of interest has been generated in the study of carbon nanoparticles, including the relative stability of sp^2-bonded and sp^3-bonded clusters [3,4].

In 1990, the quasi-one dimensional sp^2-bonded carbon nanomaterials, so called 'carbon nanotubes', were discovered [5]. Since this time, carbon nanotubes (CNTs) have already been successfully used for various applications [6], prompting speculation that other quasi-one dimensional (1-D) carbon nanostructures may also become important components in nanotechnology. In particular, nanowires are expected to play an integral role in the design and construction of both electronic and optoelectronic nanodevices [7]. Significant work has been compiled regarding the structure and properties of semiconductor nanowires including silicon [8, 9], silicon carbide [10,11] and carbon [12]. The growth of carbon nanowires has been achieved using a number of techniques including annealing of pressed tablets containing graphite [13], high pressure treatment of catalyst containing thin films [14], laser-induced chemical vapor deposition [15] and annealing of silicon carbide [16].

Diamond-based materials have been proposed as the optimal choice for nano-mechanical designs

Corresponding author: Amanda S. Barnard, e-mail: amanda.barnard@anl.gov

[17], as they possess unique structural properties such as high elastic modulus and strength-to-weight ratio [2], possibly making them ideal for structural applications at the nanoscale. However, progress in the fabrication of diamond nanowires has been limited. Preparation of diamond whiskers (a term used to describe particular type of nanowires with a strongly tapered tip) on diamond single-crystal substrates was reported as early as 1968 [18]. However, progress in this direction was not made, probably due to the difficulty of controlling the whisker dimensions. Since this time, aligned diamond nanowhiskers with a diameter of approximately 60 nm have been formed using air plasma etching of polycrystalline diamond films [19, 20], showing well-defined characteristics of diamond [20]. Diamond nanocylinders of with a diameter of approximately 300 nm have also been reported [21]. Most recently, nano-rods of single crystalline diamond have been grown [22, 23]. In general, the limited successes in the synthesis of diamond nanowires raises concerns regarding their structural and energetic viability. Are there fundamental problems that prohibit the mass production of stable 1-D sp^3 structures such as diamond nanowires?

Experimentally, it has been found that upon heating 0-D nanodiamond particles transform into carbon onions [24, 25], while the reverse transformation has been observed under electron irradiation [26-28]. This transformation has also been modelled using various levels of theory [29-32]. However, more often than not, an intermediary is formed, with a diamond-like core and an onion-like outer shell. Recent studies concerning these intermediaries, both x-ray absorption and emission measurements on nanodiamonds synthesized in detonation waves from high explosives and theoretical simulations, have suggested that a new class of carbon (so called 'bucky-diamonds') be established to describe them [33]. Such findings prompt questions as to whether similar changes in structure and hybridization observed in 0-D nanodiamond are to be expected in 1-D? Will diamond nanowires transform into single-walled nanotubes or multi-walled nanotubes?

In order to answer these questions, a number of theoretical and computational studies have been undertaken, in an attempt gain some appreciation of the relationship between nanocarbon phases (including phase stability) and to identify factors that may induce structural transformations in 1-D. To this end, theoretical studies are playing a vital role in the evolution of nanocarbon technology. Recent *ab initio* simulations of the structural relaxation of diamond nanowires with octahedral [34], dodecahedral [35] and cubic [35, 36] surface facets by Barnard *et al*. [37] found that the energetic and structural stability diamond nanowires is dependent on the surface morphology, crystallographic direction of the principle axis and nanowire diameter. A similar investigation by Erkoç and Malcioğlu [38] examined these issues using classical methods, while incorporating the effects of temperature. Using a different approach Shenderova *et al*. [39], examined the stiffness and fracture force of hydrogenated diamond nano-rods compared with those of single-walled nanotubes and multi-walled nanotubes. It was determined in this study that the mechanical properties of the nano-rods also depend on both the diameter of the nano-rod, and the orientation of the principle axis.

In this review, the current status of diamond nanowire research will be presented, including a summary of the various predictions made by theorists regarding the structure and stability of diamond nanowires, and the progress that has been made by experimentalists in this field. A short discussion will also be included considering the thermodynamic phase stability of 1-D sp^3 nanostructures, compared with CNTs. An important distinction here is the difference between carbon nanowires (CNWs), diamond nanowires (DNWs) and nano-rods (DNRs). There appears to be come confusion in the literature as to the exact definition of these terms, especially in the case of nanowire and nano-rods (which are sometimes used interchangeably). For the purposes of clarity, the term 'carbon' will be used here to refer to amorphous sp^2/sp^3 bonded structures and 'diamond' to refer to exclusively sp^3 bonded structures. Also, again for the purposes of clarity, the term 'nanowires' will be used here to refer to infinite (or 'effectively infinite', with a very high aspect ratio) structures, whereas the term 'nano-rod' will imply finite (or moderate aspect ratio) nanostructure.

2. CARBON NANOWIRES

Although the growth and structure of DNRs and DNWs is of particular interest, nanoscale materials with sp^2 and sp^3 bonds is also receiving some attention. As mentioned above, these sp^2/sp^3 material corresponds to amorphous CNWs, and contains a highly disordered network of carbon atoms that are predominantly sp^2 bonded [13], but are not hollow like CNTs. CNWs have are also being considered as the basic materials for the construction of nanometer devices [16].

A number of important studies have been undertaken to investigate various aspects of CNWs, both theoretical and experimental. A selection of contrasting studies have been chosen here for presentation, to enable the reader to appreciate the subtle differences in the growth, structure and stability of CNWs and diamond nanowires (that will be outlined in later sections).

2.1. Theoretical predictions

The structural stability of single and multi-wall zigzag CNTs have been investigated by Erkoç [40] using molecular-dynamics simulations and the Tersoff [41] empirical many-body potential energy function (PEF) developed especially for carbon. In this study, the smallest possible double and triple-wall nanotubes were considered, with results showing the multi-wall models decaying into an amorphous CNW when heat treated.

The classical Tersoff PEF [41] describes the total interaction energy of a system of particles as the sum of total two-body and total three-body contributions,

$$\Phi = \phi_2 + \phi_3 , \tag{1}$$

where, the two-body energy is given by,

$$\phi_2 = A\sum_{i<j}^{N} U_{ij}^{(1)} , \tag{2}$$

and the three-body energy given by,

$$\phi_3 = -B\sum_{i<j}^{N} U_{ij}^{(2)} \left[1+\beta^n \left(\sum_{k\neq i,j}^{N} W_{ijk} \right)^n \right]^{-\frac{1}{2n}} . \tag{3}$$

In these expressions, U_{ij} and W_{ijk} represent the two-body and three-body interactions, respectively; and A, B, β and n are among the fitting parameters, outlined in references [40] and [41].

Using the Verlet algorithm to solve the equations of motion of the carbon atoms, and the canonical (NVT) ensemble molecular-dynamics (MD) Erkoç invoked periodic boundary conditions (PBCs) along the tube axis so as to simulate infinitely long structures. Starting at low temperature (1K), the temperature of the system was increased by 300K intervals up to a maximum of 6000K. The initial velocities of the particles were determined from the Maxwell distribution at each given temperature. The simulation proceeded with $2\cdot10^5$ time steps at every temperature rise ensuring the system equilibrated at every interval.

The structure of a nanotube may be describe entirely in terms of the length and chirality. The chirality and diameter are then uniquely defined in terms of the magnitude of the components of the chiral vector $\tilde{N}_h = n\bar{a}_1 + m\bar{a}_2 \equiv (n,m)$, where n, m are integers and $\bar{a}_1$, $\bar{a}_2$ are the unit vectors of a hexagonal, graphene sheet. The particular chiralities known as 'armchair' and 'zigzag' are named for the cases where $m=n$ and $m=0$, respectively. Erkoç generated the multi-wall nanotubes (MWNTs) by nesting single-wall nanotubes (SWNTs) coaxially. The smallest diameter double-wall nanotube (DWNT) is formed from C(3,0)@(7,0)*, and the largest diameter C(7,0)@(11,0). One triple-wall nanotube was considered, formed from C(3,0)@(7,0)@(11,0). The choice of these configurations gave a separation distance between the coaxially nested nanotubes that allowed for C-C bonding between the 'walls'. As a result, the MWNTs with sizes C(3,0)@(7,0) and C(3,0)@(7,0)@(11,0) decayed by collapsing inward to form amorphous CNW during the MD simulation.

In general, it was found that the MWNTs did not withstand the heat treatment as well as SWNTs. The structure of the smaller DWNTs began to decay at 1500K, and the larger at 3900K. The C(3,0)@(7,0)@(11,0) triple-wall CNTs also began to decay at 1500K. The CNW formation was only found to be possible with small diameter MWNTs, as these structures were more able to fulfill the requirement (of a CNW) that inner part of the structure should be (at least partially) filled. The author then went on to discuss criteria based on the average coordination number of carbon atoms, and the separation distance between 'walls', that may be used as an indicator for CNW formation.

Results of further MD simulations of the structural properties of 1-D nanocarbon using the same Tersoff PEF were later reported by Erkoç and Malcioğlu [42]. In this work the authors investigated the stability of finite length CNRs, formed from open-ended isolated MWNTs with different chirality. In this case, each system was relaxed for approximately 10^5 time steps at each temperature rise, to ensure that these finite systems (with more degrees of freedom) reached equilibrium.

Once again, the CNRs were formed from the decay of MWNTs upon simulated heat treatment. Three different CNR models were considered, with varying diameters. The initial MWNTs were denoted

* The notation C(3,0)@(7,0) implies that a C(3,0) single-walled CNT is encapsulated coaxially inside a C(7,0) CNT.

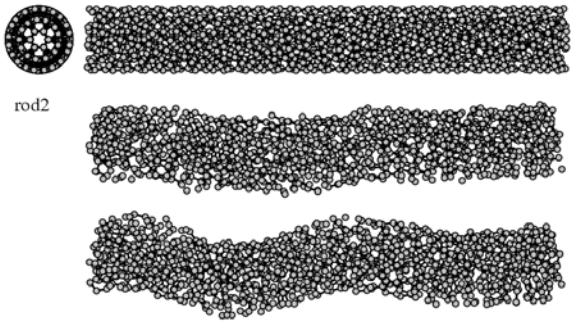

Fig. 1. Carbon nano-rod C(3,0)@(6,1)@(9,2): Ideal and relaxed structures. Reprinted from *International Journal of Modern Physics C*, Vol.13, S. Erkoç and Malcioğlu, Structural Properties of Carbon Nanorods: Molecular-dynamics simulations, p.367 © (2002), with permission from World Scientific Publishing Co. Pte. Ltd.

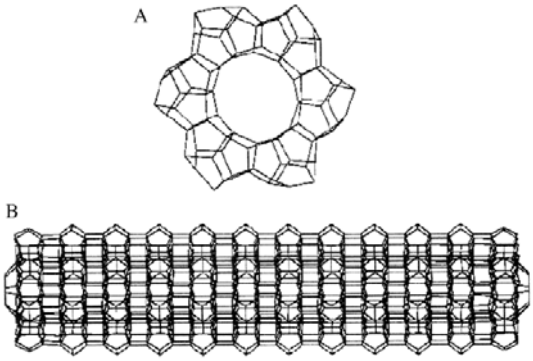

Fig. 2. (a) The "superatom" cluster containing 84 atoms (D_{6h} symmetry). Surface reconstruction results in the formation of symmetric tilted dimers. (b) A section of QOD (class 1) wire obtained by stacking the superatom units on top of each other and performing GTBMD relaxation. The ends of the segment show (111) features. Reprinted from Superlattices and Microstructures, Vol.27, M. Menon, E. Richter, P. Raghavan and K. Teranishi, Large-scale quantum mechanical simulations of carbon nanowires, p.577 © (2000), with permission from Elsevier.

as C(2;0)@(5;1)@(8;2), C(3,0)@(6,1)@(9,2) and C(4,0)@(7,1)@(10,2), respectively. Each MWNT was relaxed at low temperature (1K) to obtain their most stable structures (for approximately $1{\cdot}10^6$ MD time steps). It is important to note that in this study [42], the periodic boundary condition were not applied to the systems (as was outlined above [40]) so that these structures represent isolated finite length systems.

As an example, the initial (ideal) and final results of the C(3,0)@(6,1)@(9,2) structure are shown in Fig. 1, illustrating the decay of the MWNT (top) into the disordered CNR (bottom). It can be seen from this figure that the final structure of the CNR is no longer smooth or straight. At the end of each simulation the coordination of the atoms in the CNWs was examined, confirming the amorphous structure, since no regular coordination among the atoms could be identified.The authors do report an average coordination number of approximately 4 (sp^3-like), and an average nearest-neighbor distance of approximately 1.45 Å (sp^2-like).

Around the same time, Menon and colleagues [43] proposed a novel, physically motivated approach (supported by a quantum molecular dynamics method) to the quasi-one dimensional (QOD) structures of carbon. Although the approach was based on the premise that robust nontubular structures of carbon would be stable when constructed from a four-fold coordinated core and a three-fold coordinated surface, these structures may not be characterized as diamond nanowires and are therefore included here among other non-diamond carbon-based nanowires. Two classes of structures were proposed (class 1 and class 2), depending upon the surface to bulk ratio of atoms. The optimum (low energy) structures were determined using a generalized tight-binding molecular dynamics scheme (GTBMD) that allows for the full relaxation of covalent systems (such as carbon), with no symmetry constraints.

The GTBMD scheme of Menon and Subbaswamy [44], is characterized by a parameterized Hamiltonian (*H*) and an overlap matrix (*S*). It uses a generalized eigenvalue equation and has been previously shown to give a good description of the structural and vibrational properties of fullerenes and nanotubes [44]. It should be noted that both matrices *H* and *S* are real symmetric and sparse with sparsity increasing rapidly with the system size, thereby making the generalized eigenvalue computation intrinsically expensive (for *N*x*N* matrices, the storage requirements grow as N^2 while the number of operations grow as N^3). The QOD carbon structures were carefully relaxed to a true local minima. Assurances were also made that the vibrational frequencies had no imaginary frequencies (indicating them to be true local minima of the total energy).

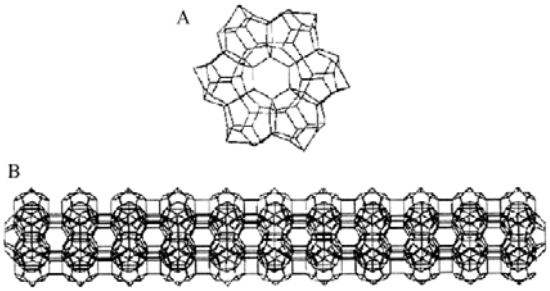

Fig. 3. (a) The "superatom" cluster unit for QOD structures belonging to (class 2). (b) A section of QCD (class 2) wire obtained by stacking the superatom on top of each other and performing GTBMD relaxation. Reprinted from Superlattices and Microstructures, Vol.27, M. Menon, E. Richter, P. Raghavan and K. Teranishi, Large-scale quantum mechanical simulations of carbon nanowires, p.577 © (2000), with permission from Elsevier.

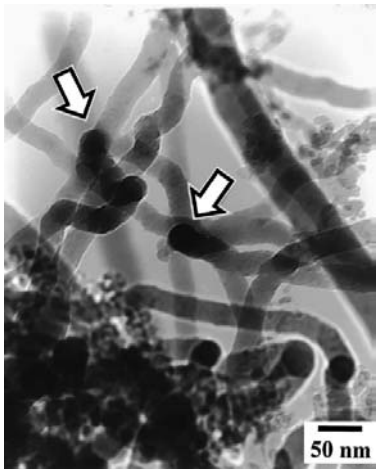

Fig. 4. TEM micrograph of the cross section of the nanowires, with arrows indicating the nanowire cross sections at the turning points as the nanowires change their growth directions. Reprinted from Applied Physics Letters, Vol.75, Y. H. Tang, N. Wang, Y. F. Zhang, C. S. Lee, I. Bello and S. T. Lee, Synthesis and characterization of amorphous carbon nanowires, p.2921 © (1999), with permission from American Institute of Physics.

The building blocks for class 1 QOD structures are multiply connected 'superatom' clusters having D_{nh} symmetry with a hollow (tubular) region through the center. Fig. 2a shows a representative structure with D_{6h} symmetry. This superatom C_{84} cluster can be visualized as consisting of six circularly connected closed units, each with 14 atoms, and with faces composed of pentagons and hexagons. In this case, 60 atoms have three-fold coordination, and remaining atoms are all four-fold coordinated. The bonding of the atoms at the top and bottom, along the symmetry axis to their three neighbors resemble the unreconstructed (111) surface of diamond. The atoms on the surface farthest from the symmetry axis form dimers as a result of the (2x1) reconstruction, but the unreconstructed surface resembles the (100) surface of diamond.

The QOD structure obtained by stacking these clusters along the symmetry axis is shown in Fig. 2b, consisting of 1020 atoms. The stacking results in four-fold coordination for all the C(111)-like atoms, but the surface dimers remain three-fold coordinated and do not form bonds with atoms in the neighboring unit cells. The authors note, however, that this structure is only locally stable.

Class 2 structures examined by Menon *et al.* [43] were characterized by smaller surface-to-bulk ratios, with a superatom unit consisting of 90 atoms. This structure, as shown in Fig. 3a, was obtained by adding a ring of six C atoms around the symmetry axis of a class 1 unit structure. The corresponding rod-like structure generated by stacking this class 2 superatom unit (Fig. 3b) was also found to be locally stable, although the structure belonging to class 2 was found to be more stable than that belonging to class 1.

The authors therefore concluded that QOD structures of this type may be stable, provided that their geometries consist of a core of four-fold coordinated atoms surrounded by a three-fold coordinated outer surface [44]. Although not a true diamond nanowire, this study does provide useful insight into the possible structure of CNWs, especially in the cases where experiments identify both sp^2 and sp^3 bonding.

2.2. Experimental progress

Although not as prevalent as the sp^2 bonded counterparts, sp^2/sp^3 bonded CNWs have been grown experimentally using various techniques. The structural characteristics and mechanical properties of these nanomaterials are still not fully understood, and much of the research to date has centered on the growth techniques and the dependence of CNW growth on experimental parameters such as catalyst and temperature.

Tang *et al.* [13] have reported the successful synthesis of CNWs by a thermal evaporation technique and annealing of pressed tablets containing graphite, described in detail in reference [13]. The diameters of most of the nanowires are around 40 nm (although some were as low as 10 nm). The CNWs were positively identified using Raman spectroscopy and selected-area electron diffraction (SAED) patterns of an individual nanowire, confirming that the nanowires were not crystalline. A scanning electron microscope (SEM) micrograph of the CNWs is show in Fig. 4. Unlike carbon fibers and diamond nanowires, amorphous nanowires of this type are smooth and curvy. As the nanowires change their growth directions, their cross section can be observed at the turning points which are marked by arrows in Fig. 4. It can be seen from the image that the nanowires have a circular, solid cross section.

In their study, Tang and colleagues determined that metallic catalysts (Ni) played an important role in the growth of the nanowires; indeed the CNWs could not be formed without Ni [13]. It was also found that the diameters of the nanowires were dependent on the concentration of Ni powder in the tablet, and that when the concentration of Ni was high enough (1 wt.%) irregular shaped nanoparticles (composed of C and Ni as detected by energy-dispersive X-rays) were observed on the tips of the nanowires. When the concentration of Ni in the graphite powder was below 1 wt.%, the authors reported nanowires of a smaller diameter.

A CO-assisted growth model of carbon nanowires is proposed in this work, in which graphite reacts first with the oxygen or water trapped within the tablet at high temperature:

$$2C+O_2 \rightarrow 2CO, \quad (4)$$

and

$$C+H_2O \rightarrow CO+H_2. \quad (5)$$

Argon gas was used to carry the CO molecule to the colder growing nanowire where it decomposes into graphitic atoms and carbon dioxide molecules at the surface of the metallic catalyst:

$$2CO \rightarrow C+CO_2. \quad (6)$$

The gaseous CO_2 was then evacuated by the mechanical pump. Further details on this growth model may be found in reference [13].

In a later study, Lui *et al.* [14] examined the use of three different catalyst materials for the growth of CNWs, including Ni thin films, Ni-containing diamond-like carbon (Ni-DLC), and Co thin films. The cobalt thin films were prepared using a MBE technique, to a thickness of 25 nm. The nickel thin films (of varying thickness) were deposited using dc sputter deposition technique, and the Ni-DLC thin films were obtained using a radio frequency (RF) reactive sputter deposition technique. The deposition conditions were varied such that films with different amounts and sizes of Ni nano-particles (as well as other characteristics) were obtained, as described in reference [14]. A MPCVD system was used to grow the and CNWs under mixtures of methane and hydrogen. Growth parameters, including pressure, microwave power, and methane concentration, were varied during the study, and the resulting specimens examined using low angle X-ray diffraction (XRD), transmission electron microscopy (TEM) and SEM.

CNWs were obtained using catalysts of Ni thin films, but not in the case of Co thin film or Ni-DLC thin films catalysts. The results of their investigations show various amounts of CNTs and CNWs, depending on the thickness of the catalyst. When 18 nm thick amorphous Ni catalysts were used it was also found that the formation of CNW depends on the pressure. For example, at a pressure $\leq 3.33 \cdot 10^3$ Pa CNTs predominated; however, at a pressure $>3.33 \cdot 10^3$ Pa only limited amounts of CNWs were observed. Similar trends were observed when using 286 nm thick polycrystalline Ni as the catalyst. Both single and multiple CNWs were reported. Typical diameters of single CNWs were <10 nm, and the graphene planes in multiple CNWs were oriented perpendicular to the wire axis.

Botti *et al.* [15] described an alternative, efficient fabrication route of tubular carbon nano-structures, using amorphous hydrogenated carbon nano-particles as precursor, without metal catalyst addition. They succeeded in producing carbon nanowires with mean diameter of 250 nm, formed by low-velocity spraying of carbon particles onto a heated Si(100) substrate, when the deposition temperature is sufficiently high to enable self-assembling processes. Both the diameter and the structure of carbon fiber were found to vary, depending on reaction conditions.

The carbon nano-particles were prepared in a flow reactor from an ethylene-acethylene mixture by laser-induced chemical vapor deposition. After synthesis, the nano-particles were charged in a reservoir, mixed with a gas carrier and introduced into the deposition chamber, through a pipe system. The particles were passed through a nozzle, accelerated to approximately 30 m/s and then deposited by impaction onto a heated substrate for film formation. The morphology and structure of the carbon

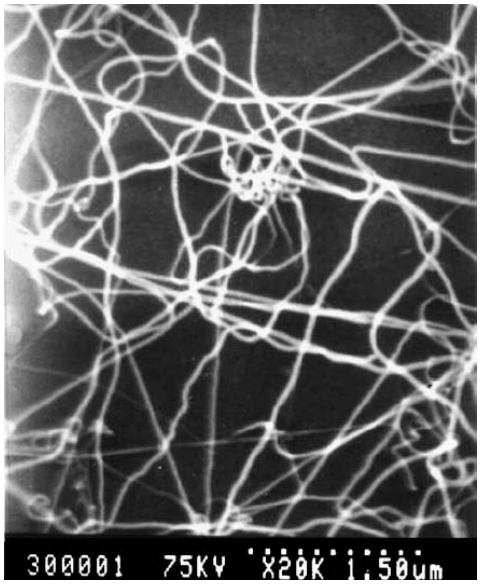

Fig. 5. The SEM micrograph CNWs on the sample after annealing at 1150 °C for 3 hours in H_2 ambient. Reprinted from Applied Surface Science, Vol.193, A. Xia, Z. Huizhao, Y. Li and X. Chengshan, Formation of carbon nanowires by annealing silicon carbide films deposited by magnetron sputtering, p.577 © (2000), with permission from Elsevier.

films were characterized using SEM, Raman spectroscopy and reflection high-energy electron diffraction (RHEED).

Although the main thrust of the research of Botti *et al.* [16] was the non-catalyst assisted growth of CNTs, by using deposition times up to 90 min, a high density of CNWs with a diameter of 250±80 nm laid down on the substrate, with 'long noodle shapes'. Most of the carbon nanowires are smoothly curved with some short straight sections, while some possess many kinks and bends. Experimental procedures, growth mechanisms and characterization measurements are outlined by the authors, in comparison to carbon nanotubes grown using the same technique [15]. These results illustrate how CNTs and CNWs may be grown under similar conditions, with only relatively minor modifications necessary to grow the desired carbon nanostructure.

Finally, using yet another approach, Xia and colleagues [16] presented the first successful formation of carbon nanowires, prepared by RF magnetron sputtering, using an n-type Si(111) wafer as a substrate and ceramic silicon carbide as sputtering target. Once a stable chamber pressure was achieved, the RF generator was set to 150 W for the purposes of sputtering. During this time the target holder was used as the cathode and the substrate as the anode, separated by 80 mm. Silicon carbide films with a thickness of ~1100 nm were deposited on the Si substrate at room temperature, at a rate of ~550 nm/h. Subsequently, the sample was placed on a quartz carrier and was annealed in an open tube furnace. Fourier transform infrared transmission spectroscopy (FTIR), X-ray photoelectron spectroscopy (XPS) analysis, XRD and SEM microscopy were then used in the characterization of the samples.

After annealing, many CNW structures were observed on the surface of the film (see Fig. 5). The diameters of the nanowires were not uniform (between 20 and 60 nm), with an average length of 8 to 9 μm. Some nanowires were observed over 10 μm in length. Although it is the topic of ongoing research [17], the authors speculate that the formation mechanism of the carbon nanowires is related to hydrogen reduction resulting in an excess C atoms formed by the collision of SiC with Ar^+ during the sputtering process. Thus it was shown that carbon nanowires can be formed at the temperature of 1000 °C or higher, during H_2 annealing [16].

3. DIAMOND NANOWIRES

With the expansion of nanotechnology surrounding CNTs, the next logical step in the study of nanocarbon is the investigation of DNWs and DNRs. As mentioned above, the numerous theoretical and computational studies of the phase stability of 0-D carbon nanoparticles indicate that this topic is undoubtedly non-trivial. Never the less, there have been far fewer studies regarding the stability of diamond nanowires. In order to predict the structural properties of diamond nanowires, to evaluate their suitability for structural applications, and to ascertain if such structures are stable (or whether conversion to SWNTs or MWNTs will ensue), it is important to gain an appreciation of the effects of various surfaces and growth directions on their stability.

3.1. Theoretical predictions

Since it is the C(111) surface that has been shown to be unstable on the surfaces of diamond nanocrystals, exhibiting preferential exfoliation over lower index surfaces [30, 32], we will begin by summarizing theoretical studies examining the stability of the C(111) surface on diamond nanowires.

The stability of dehydrogenated C(111) and hydrogenated C(111):H surfaces on diamond nanowires

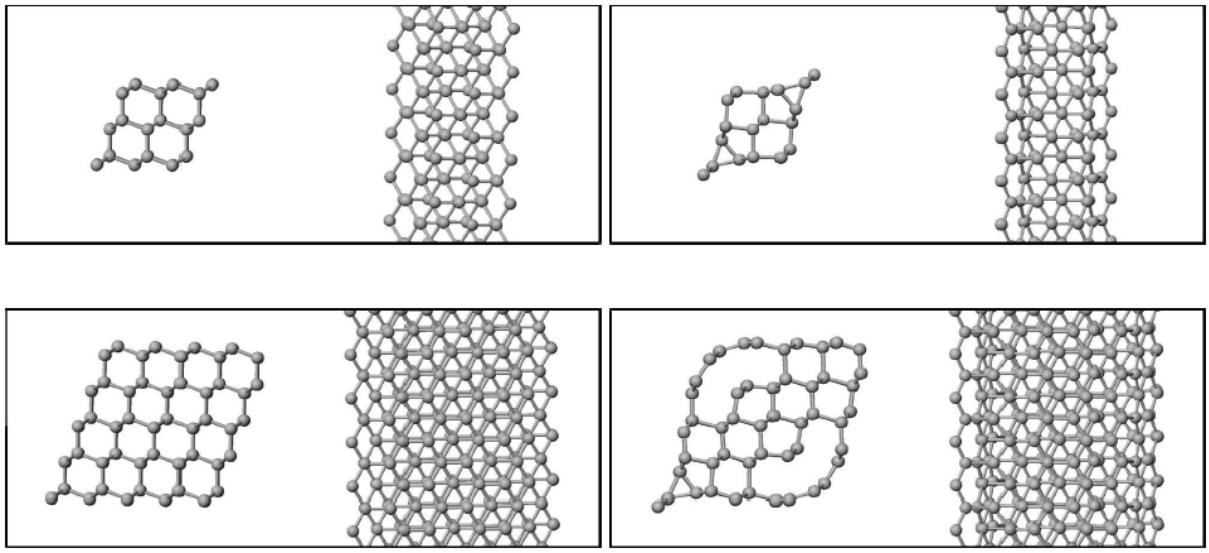

Fig. 6. Initial (left panels) and relaxed (right panels) structure of the 0.43 nm (top) and 0.90 nm (bottom) octahedral DNWs investigated by Barnard *et al.* [35]. In each panel, the DNWs are shown parallel (left) and perpendicular (right) to the principle axis. Courtesy A. S. Barnard.

was investigated by Barnard *et al.* [34], using two nanowire morphologies. The calculations in this study was performed with the Vienna *ab initio* simulation package (VASP) [45, 46] using ultra-soft, gradient corrected Vanderbilt-type pseudopotentials (US-PP) [47, 48] and a plane wave basis set which spans reciprocal space with a plane-wave basis up to a kinetic energy cutoff of 290 eV. The crystal relaxations were performed in the framework of Density Functional Theory (DFT) within the Generalized-Gradient Approximation (GGA), with the exchange-correlation functional of Perdew and Wang (PW91) [49]. The Linear Tetrahedron Method (LTM) with a 4x4x4 Monkhorst-Pack *k*-point mesh was used for the Brillouin zone integration. Although this choice of *k*-mesh results in some superfluous *k*-points (in non-periodic directions perpendicular the nanowire axis), it was found that the inclusion of these *k*-points is more consistent with the LTM and assisted in converegence of the [50].

The two morphologies were characterized by octahedral and cuboctahedral lateral forms, with the nanowire principle axis in the [110] direction. The octahedral nanowires structures were bounded by {111} surfaces in all directions perpendicular to the axis direction (with a rhombohedral cross-section), and the cuboctahedral DNWs by four C(111) and four C(100) surfaces with an almost circular cross-section. All of their initial structures have been 'cleaved' from a bulk diamond lattice, with both C(111)(1x1) single dangling bond and C(100)(1x1) double dangling bond surface structures. PBCs were applied in the direction of the principle axis, to create infinite structures. The hydrogenated nanowires were obtained by saturating all dangling bonds with a H atom (giving a coverage of $\theta = 1$). Examples of the initial (ideal) and final (relaxed) structures are shown in Figs. 6 and 8 (viewed perpendicular and parallel to the DNW axis) for the octahedral and cuboctahedral structures, respectively.

The authors reported a very unusual relaxation for the octahedral diamond nanowires, involving the formation of 3-membered rings at the acute 60° edges. For example, the C(111) surfaces of the smallest octahedral diamond nanowire (with an average lateral diameter of 0.43 nm) was found to relax inward, in complete opposition to the exfoliation observed in the octahedral nanodiamonds, adopting a concave shape when viewed in cross-section. This unusual shape was attributed to the formation of dimers in the [100] direction (denoted as '[100] dimers') just below the acute nanowire edges, even in the absence of a C(100) surface facet. The formation of 3-membered rings is highly unusual, however the reported final energy per atom of -6.678eV was significantly lower than the reported initial energy per atom of -6.307eV.

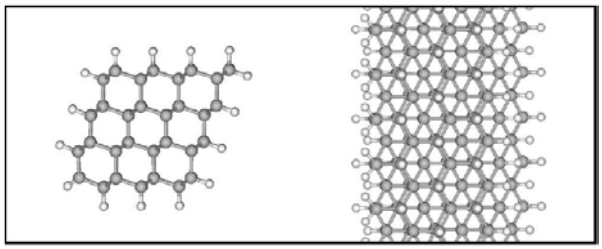

Fig. 7. The structure of the relaxed 0.68 nm hydrogenated octahedral DNW investigated by Barnard [35]. In each panel, the DNWs are shown parallel (left) and perpendicular (right) to the principle axis. Courtesy A. S. Barnard.

In the case of larger dehydrogenated octahedral DNWs the formation of '[100]-dimers' along one (acute) edge of the nanowire was also observed, again resulting in a row of 3-membered rings. In these cases however, the authors report that C(111) surfaces (above the [100]-dimers) become unstable, and exfoliated to form nanotubular-cages orientated parallel with the nanowire principle axis. These tubular-cages had a chiral structure identical to that of an armchair CNT, and remained attached to the inner diamond-like core of the nanowire as shown in the lower panel of Fig. 6. The inner diamond core also contracted, giving a cage-core separation distance of ~2.52-2.57 Å.

In the case of the cuboctahedral DNWs, Barnard *et al.* [34] reported that the first step of the relaxation involved reconstruction of the C(100) surfaces to the C(100)(2x1) structure, followed by exfoliation of the C(111) surfaces. The relaxation of the smallest (0.42 nm) cuboctahedral DNW included in their study resulted in the entire nanowire transforming into a 'non-classical' nanotube, with the core atoms forming an sp bonded linear chain along the axis. The authors denoted this structure as a non-classical nanotube, since the armchair structured sections (formed by the exfoliation of the C(111) surface) were separated by rows of 8-membered and 5-membered rings, which are not present in classical CNTs (see the top panel of Fig. 8). A linear chain of this type has been observed in the center of MWNTs experimentally [51].

Similarly, the C(111) surfaces of the larger (0.63-0.83 nm) cuboctahedral nanowires were also found to exfoliate (following the C(100) reconstruction), forming nanotubular-cages on the surface oriented parallel to the principle axis. Like the dehydrogenated octahedral DNWs mentioned above, the nanotubular-cages remained bound to the inner core atoms at the C(100)(2x1) surfaces, and the inner core of the cuboctahedral nanowires contracted resulting in a cage-core separation distance of approximately 2.42-2.54 Å. The final structure of the largest 0.83 nm cuboctahedral diamond nanowire is shown in Fig. 9, viewed from the [100] and principle axis directions.

Barnard *et al.* also explicitly listed a number of structural characteristics of the (initial and) final relaxed diamond nanowires, such as expansions and/or contractions of the nanowire segments. The pa-

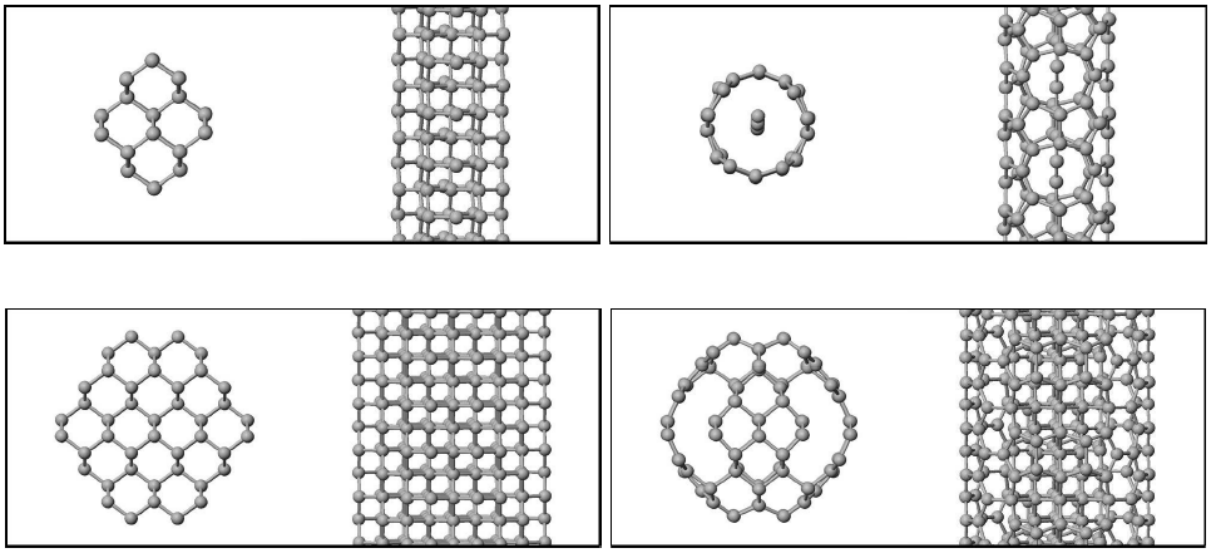

Fig. 8. Initial (left panels) and relaxed (right panels) structure of the 0.42 nm (top) and 0.83 nm DNWs investigated by Barnard *et al.* [35]. In each panel, the DNWs are shown parallel (left) and perpendicular (right) to the principle axis. Courtesy A. S. Barnard.

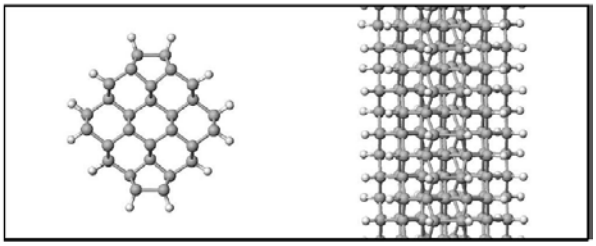

Fig. 9. The structure of the relaxed 0.63 nm hydrogenated cuboctahedral DNW investigated by Barnard [35]. In each panel, the DNWs are shown parallel (left) and perpendicular (right) to the principle axis. Courtesy A. S. Barnard.

per concluded that the C(111) nanocrystalline diamond surfaces of these structures are not stable in 1-D, due to the delamination of the C(111) surfaces upon relaxation. The resulting nanowires, characterized by (armchair) nanotubular-cages along the surface, and diamond-like cores were denoted as 'bucky-wires', as they represented the 1-D analogue of the bucky-diamonds, formed by the exfoliation of octahedral surface facets on 0-D diamond nanocrystals.

In all cases, the authors took great care in ensuring that these bizarre shapes were not metastable, intermediary structures (on the way to a more stable and energetically preferred morphology), by perturbing the structures and extending the simulation as necessary. It is also important to note that in each case, these instabilities were eliminated by surface hydrogenation. None of the unusual [100]-dimer formation or C(111) surfaces delamination were observed when the surfaces of the nanowires were H-terminated as shown in Figs. 7 and 9.

Barnard and colleagues did find however that certain diamond structures are stable in 1-D [35, 37]. The results described above were complemented by an investigation of three alternative nanowire morphologies (as a function of size), characterized by pure dodecahedral forms and combinations of cubo-dodecahedral forms. This choice of morphologies succeeded in avoiding the unstable octahedral surfaces, while still offering a range of cross-sections and surface structures. Once again, the initial structures were cleaved from a bulk diamond lattice, PBCs were applied along the principle axis to create infinite 1-D structures, and each nanowire was relaxed using DFT GGA methods [35].

The dodecahedral nanowires were bounded by {110} surfaces in all lateral directions (with a square cross-section), and had a [100] principle axis. Examples of the final dodecahedral diamond nanowires are shown in Fig. 10. Although the outermost atomic layer was found to contract inwards, no surface exfoliation, reconstruction or buckling was reported. The outer-most atomic layer contraction was found to be more pronounced at the nanowire edges, causing the {110} surfaces to adopt a slightly convex shape. This convex surface shape was not observed in the case of the hydrogenated dodecahedral nanowires. An example of the hydrogenated structures are shown in Fig. 11.

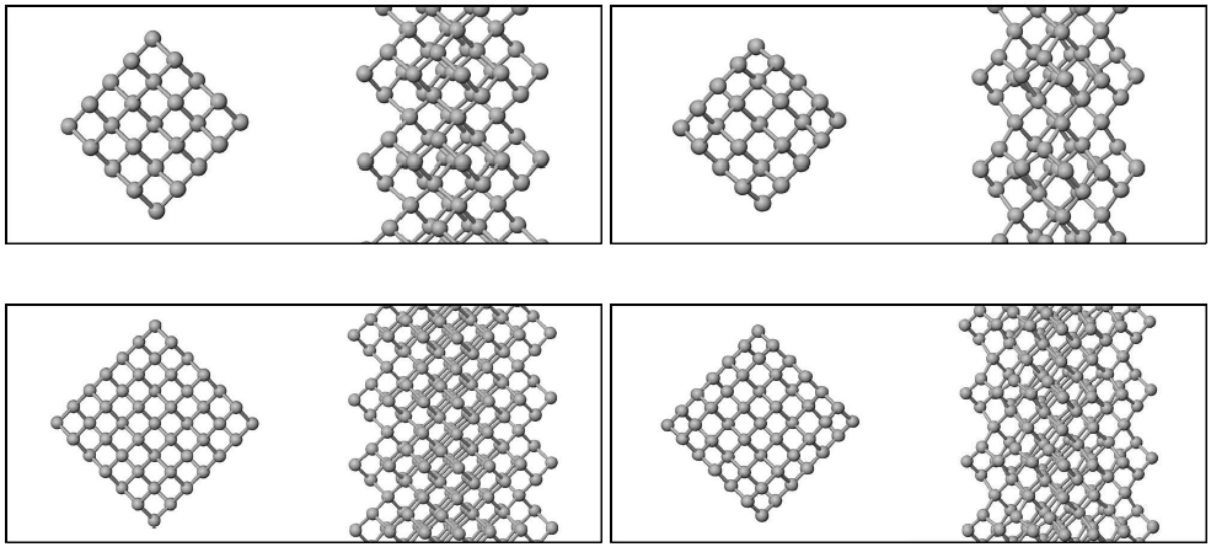

Fig. 10. Initial (left panels) and relaxed (right panels) structure of the 0.46 nm (top) and 0.72 nm (bottom) dodecahedral DNWs investigated by Barnard *et al.* [36]. In each panel, the DNWs are shown parallel (left) and perpendicular (right) to the principle axis. Courtesy A. S. Barnard.

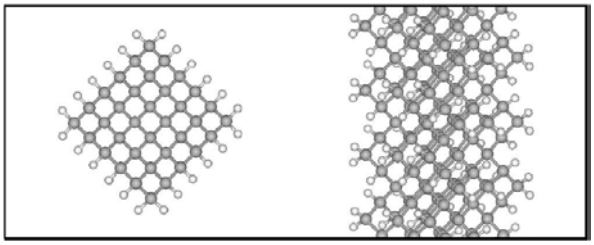

Fig. 11. The structure of the relaxed 0.63 nm hydrogenated dodecahedral DNW investigated by Barnard [51]. In each panel, the DNWs are shown parallel (left) and perpendicular (right) to the principle axis. Courtesy A. S. Barnard.

In this study, one of the cubo-dodecahedral morphologies was termed 'cylindrical' due a quasi-circular cross-section (see Fig. 12). The cylindrical DNWs were bounded by four C(100) surfaces and four C(110) surfaces and had a [100] principle axis. The authors describe the relaxation of the cylindrical nanowires involving the reconstruction of the C(100) surfaces to form the C(100)(2x1) surface structure, followed by further relaxation of the entire nanowire. The final relaxed cylindrical nanowires were also shown to a have a twisted rope-like structure, resulting from the C(100)(2x1) surface reconstruction and significant contraction of the outer most atomic layer [35]. Although less pronounced, this rope-like structure persists when the nanowire surfaces were H-terminated.

The other cubo-dodecahedral morphology was termed 'cubic', and was bounded by two C(100) surfaces and two C(110) surfaces with a square/rectangular cross-section and [110] principle axis (see Fig. 14). The authors reported [36] that each of the cubic DNWs underwent a two-stage relaxation, in which the initial stage involved the reconstruction of the C(100) surfaces to form the C(100) (2x1) surface structure. This was followed by further relaxation of the entire DNW. Upon relaxation the smallest cubic DNW (with a diameter of <0.5nm) transformed into a 'non-classical' SWNT; a transition which involved the dissociation of dicarbon molecules from the surface. This instability was however eliminated when the surfaces were H-terminated, as shown in the top panel of Fig. 15.

An example of the larger, structurally stable cubic DNW is shown in the lower panel of Fig. 14. This 0.81 nm cubic structure reportedly adopted a slightly tapered cross-section (but the bulk-diamond sp^3 structure was preserved), with C(100)(2x1) dimers comparable to bulk-diamond surfaces [36]. A more detailed characterization of the C(100)(2x1) surface structure of the cubic diamond nanowires (including the structure shown in the lower panels of Figs. 14 and 15) was also outlined by Barnard *et al.* [36], explicitly comparing the DNW surface with the corresponding nanodiamond and bulk-diamond surfaces. This study compared various surface bond lengths and atomic layer relaxation depths, as a function of the direction of the surface dimer rows

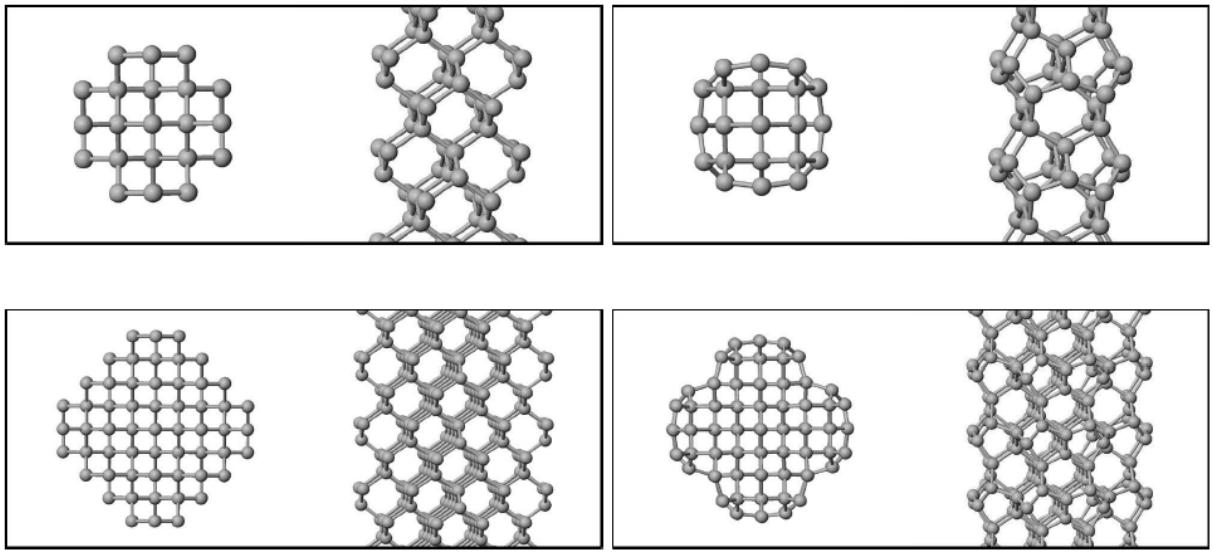

Fig. 12. Initial (left panels) and relaxed (right panels) structure of the 0.43 nm (top) and 0.84 nm (bottom) 'cylindrical' DNWs investigated by Barnard *et al*. [36]. In each panel, the DNWs are shown parallel (left) and perpendicular (right) to the principle axis. Courtesy A. S. Barnard.

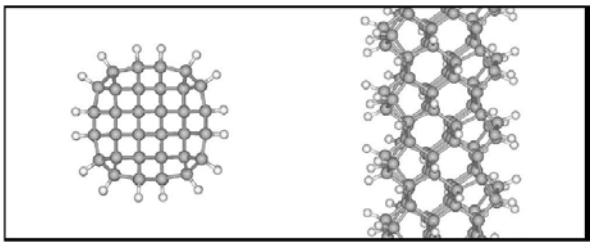

Fig. 13. The structure of the relaxed 0.61 nm hydrogenated 'cylindrical' DNW investigated by Barnard [51]. In each panel, the DNWs are shown parallel (left) and perpendicular (right) to the principle axis. Courtesy A. S. Barnard.

and the position of the surface dimers with respect to the nanowire edges.

The study found that, although a considerably degree of variation in surface structure exists due to the nanowire edges, this variation was reduced by surface hydrogenation. By comparing results for surfaces with dimer rows oriented both parallel and perpendicular to the nanowire axis, it was determined that dehydrogenated DNWs should ideally be constructed with C(100)(2x1) dimer rows parallel to the principle axis, but hydrogenated DNWs with dimer rows perpendicular to the nanowire axis [36].

Hence (with exception of the smallest cubic nanowire), the diamond structure was preserved in all of the dehydrogenated dodecahedral and cubo-dodecahedral nanowires upon relaxation. The authors also outlined secondary relaxations, involving changes in the cross-sectional area and length of the nanowires (considered in terms of the extension or contraction of the segment length within the simulation cell), which indicated that the [100] axis direction may be preferential to the [110] direction [36]. Overall, the relative stability (characterized by the variation in these structural properties from that of bulk-diamond), was found to be dependent on both the surface morphology and the crystallographic direction of the principle axis [38].

Following on from their previous work on the structural stability of SWNT, MWNTs and CNWs (described above) Malcioğlu and Erkoç [39] have studied the stability of diamond nanowires of different diameters and different crystal orientations under heat treatment by means of molecular-dynamics simulations. Once again, the Tersoff PEF [42] was used in the calculations (see above), and PBCs were applied in the direction of the nanowire axis to produce infinite structures. Beginning with the smallest possible nanowire structure for each of the low index (001), (110) and (111) surfaces of diamond the authors generated nanowires with different sizes (cross-section), and principle axes perpendicular to the corresponding surface (e.g. the {001} DNWs had principle axes in the [100] direction, *etc*). Hence the principle axis was in a crystallographic equiva-

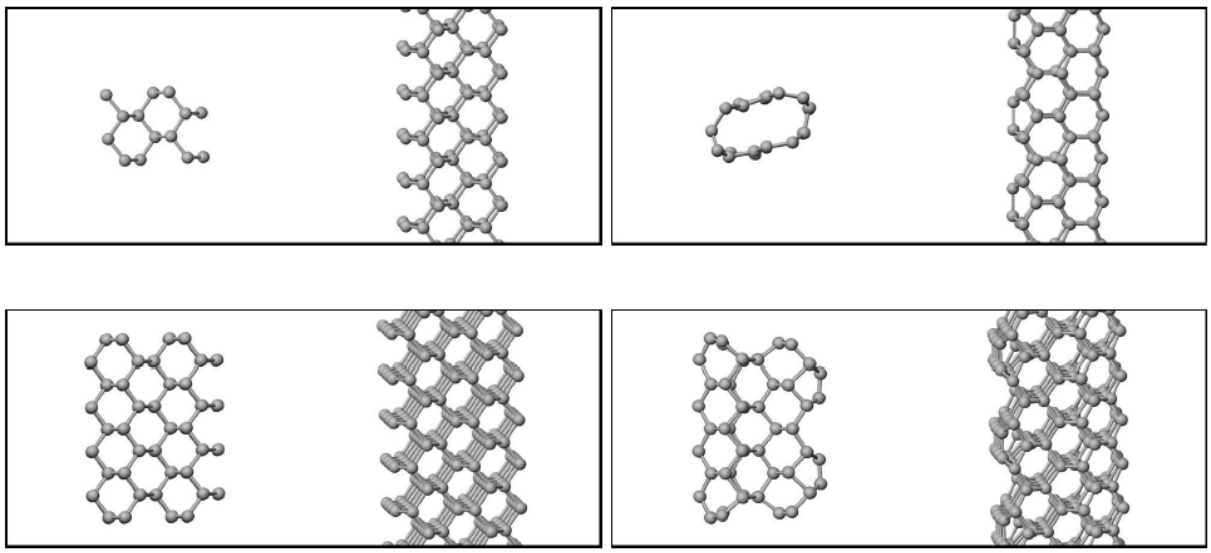

Fig. 14. Initial (left panels) and relaxed (right panels) structure of the 0.45 nm (top) and stable 0.81 nm (bottom) 'cubic' DNWs investigated by Barnard *et al*. [36]. In each panel, the DNWs are shown parallel (left) and perpendicular (right) to the principle axis. Courtesy A. S. Barnard.

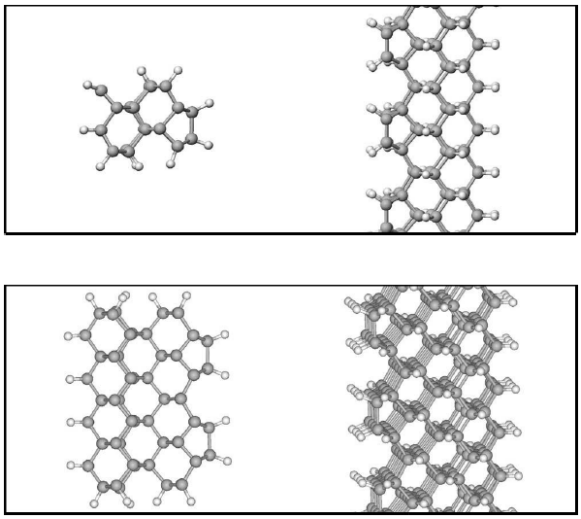

Fig. 15. The structure of the relaxed 0.43 nm (left panel) and 0.82 nm (right panel) hydrogenated 'cubic' DNWs investigated by Barnard *et al.* [37]. In each panel, the DNWs are shown parallel (left) and perpendicular (right) to the principle axis. Courtesy A. S. Barnard.

lent direction to the surface normals (unlike the DNWs of Barnard *et al.* [34, 35] where the direction of the axis was in some cases in a different crystallographic direction that the surface normals).

The simulations were carried out beginning at a temperature of 1K, and proceeded until the structure became significantly distorted. The temperature was increased with steps of 100K, and system relaxed for approximately $5 \cdot 10^5$ time steps at each temperature interval. The relative temperature at which the required degree of distortion was observed was used as the measure of stability. The authors used the average coordination number as an indicator of size, since the coordination number is proportional to the surface to volume ratio of the DNWs, and hence the diameter. The results of this study indicated that the stability of the diamond nanowires under high temperature conditions show a dependence on both the crystal surfaces present, and on the orientation of the principle axis (cross-sectional geometry).

In Fig. 16, the initial (ideal) and relaxed geometries of the {111} nanowires are shown, indicating the temperature at which the structures reached the required degree of distortion [38]. The model M1 {111} was found to be extraordinarily stable under heat treatment, maintaining the structure until 6800K without fragmenting. Surprisingly, the larger M2 and

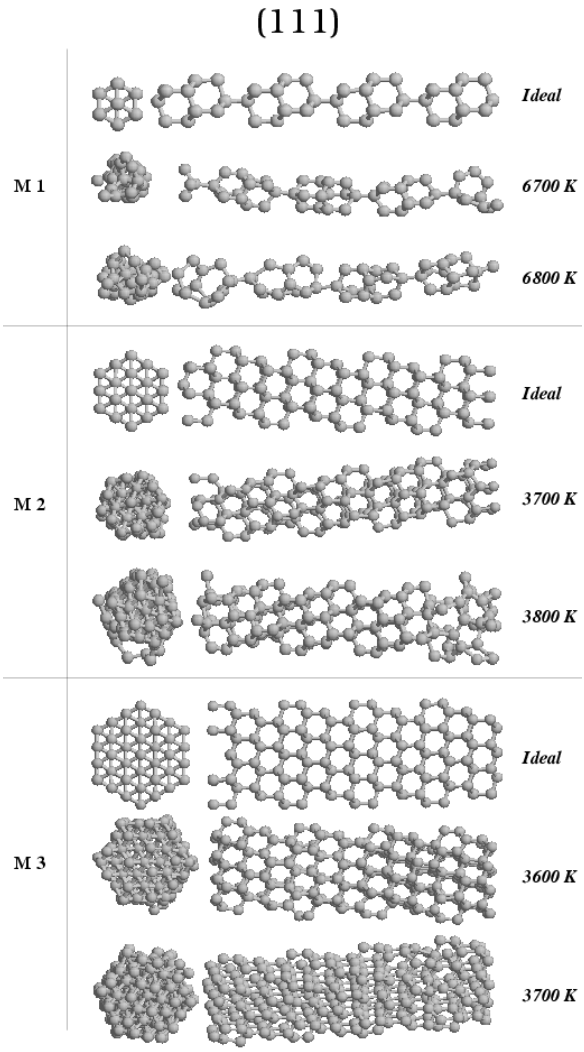

Fig. 16. Diamond nanowires generated perpendicular to the (111) surface. Three models were considered (M1, M2 and M3). The diagrams show cross-section (left) and side views (right) of the ideal and relaxed structures at various temperatures. Reprinted from International Journal of Modern Physics C, Vol.13, O. B. Malcioğlu and S. Erkoç, Structural Properties of Diamond Nanorods: Molecular-dynamics simulations., p.441, © (2003), with permission from World Scientific Publishing Co. Pte. Ltd.

M3 {111} models were found to be less stable with respect to the model M1.

This situation appears reversed in the case of the {001} DNWs, as an increase in stability with coordination number was observed as indicated by Fig. 17. The authors highlight that although the volume decreases slightly in model M3 {001}, due to larger coordination number, M3 is more stable than M2 under heat treatment.

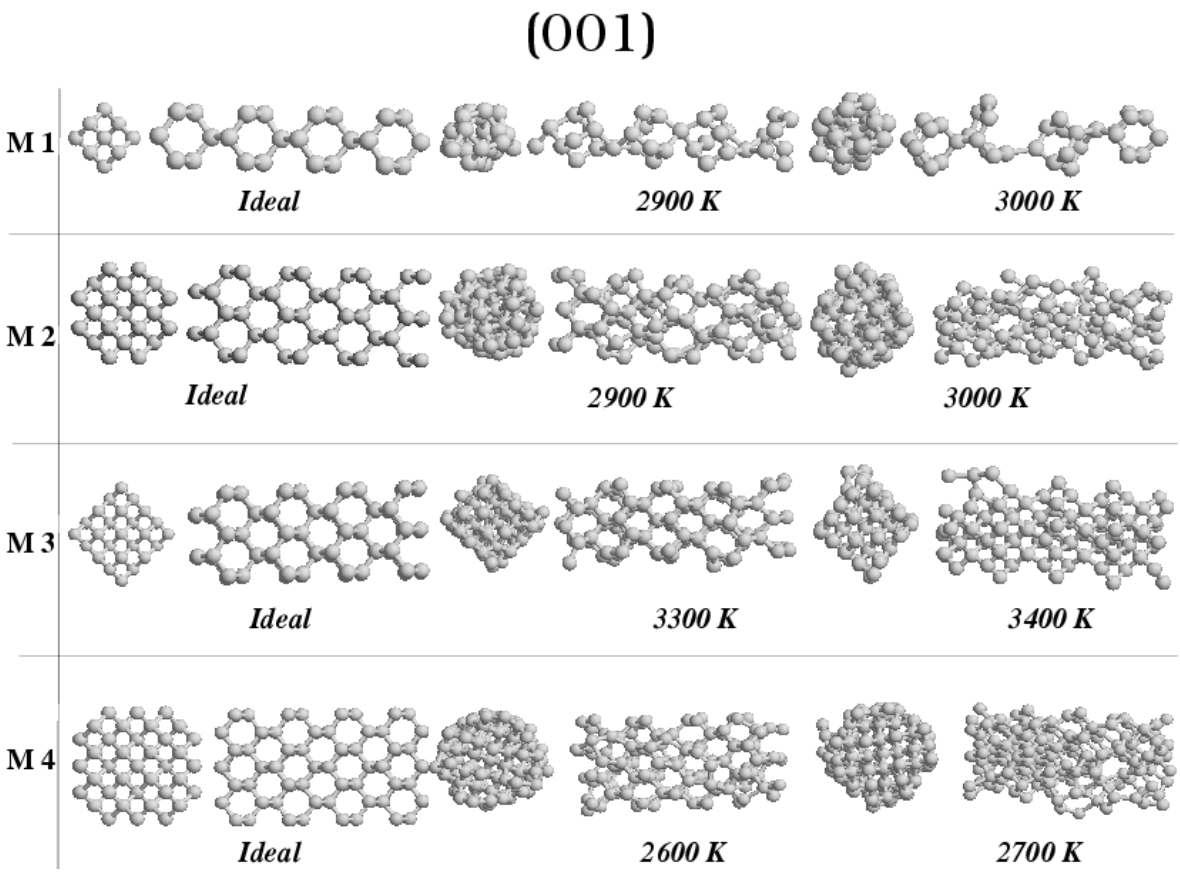

Fig. 17. Diamond nanowires generated perpendicular to the (001) surface. Three models were considered (M1, M2, M3 and M4). The diagrams show cross-section and side views of the ideal and relaxed structures at various temperatures. Reprinted from International Journal of Modern Physics C, Vol.13, O. B. Malcioğlu and S. Erkoç, Structural Properties of Diamond Nanorods: Molecular-dynamics simulations., p.441, © (2003), with permission from World Scientific Publishing Co. Pte. Ltd.

Finally, Fig. 18 shows the initial and relaxed geometries of the {110} nanowires. The authors describe the relaxed structures of the M2 and M3 {110} as becoming two-dimensional (planar) structures (and therefore unstable), due to their cross-section geometry. They also determined that the configuration of the atoms in the M4 {110} structure promotes stability, pointing out that the M4, M6 and M7 {110} structures (which all contain this configuration) are considerably more stable than the M5 {110} model (which does not).

In general, the nano-rod models with larger coordination number and suitable cross-section geometry were found to be more stable under heat treatment. Although the claim is made that the stability of the M1 {111} DNW is the most stable one [38], it is the opinion of the present author that this statement is misleading, as it suggests that the {111} group is the most stable, even though the M1 {111} is clearly not representative of this group. The next most stable DNW proposed by Erkoç and Malcioğlu is M4 {110} structure. Overall Erkoç and Malcioğlu conclude that the stability of DNWs considered in this study is highly dependent upon the cross-section geometry, average coordination number, and crystallographic orientation of the surface facets [38].

The dependence of DNW properties on the direction of the principle axis is not limited to the structural stability, but has also been found to influence the mechanical properties. It has been shown by Shenderova *et al.* [39] that DNRs with [100] principle axes show increased structural stability and enhanced mechanical properties over nano-rods with alternative growth directions. In this study, the mechanical properties of SWNTs and MWNTs were

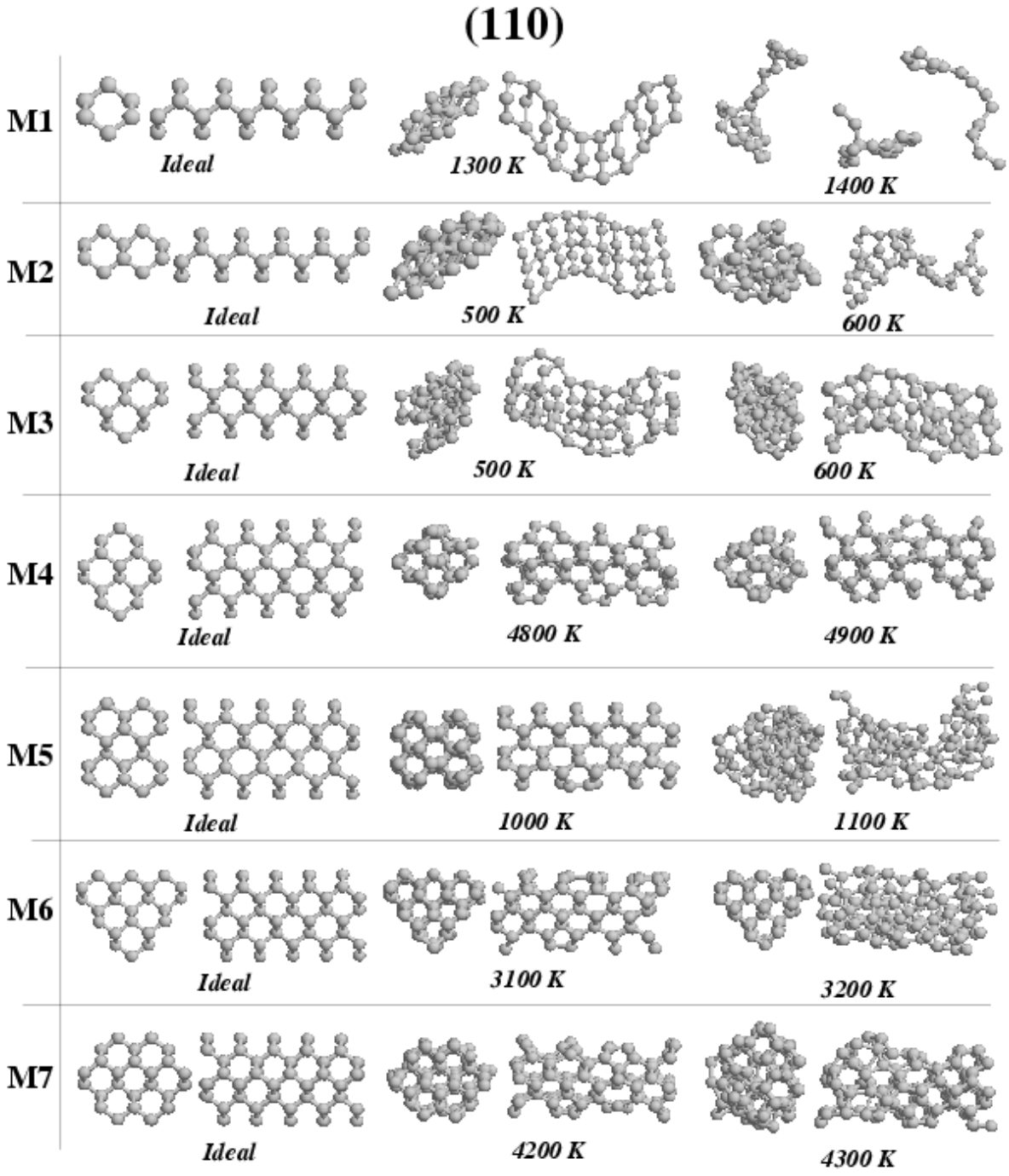

Fig. 18. Diamond nanowires generated perpendicular to the (110) surface. Three models were considered (M1 to M7). The diagrams show cross-section (left) and side views (right) of the ideal and relaxed structures at various temperatures. Reprinted from International Journal of Modern Physics C, Vol.13, O. B. Malcioğlu and S. Erkoç, Structural Properties of Diamond Nanorods: Molecular-dynamics simulations., p.441, © (2003), with permission from World Scientific Publishing Co. Pte. Ltd.

compared to the predicted properties of equivalent DNRs. The study illustrated that above a critical radius of approximately ~1-3 nm the force needed for brittle fracture of a diamond nanowire exceeds that of an equivalent SWNT, and the zero strain stiffness of diamond nanowires will exceed that of SWNTs for radii greater than ~ 1 nm. The higher fracture force was attributed to the larger load-bearing cross-sectional area of diamond nanowires compared to SWNT (with the same diameter).

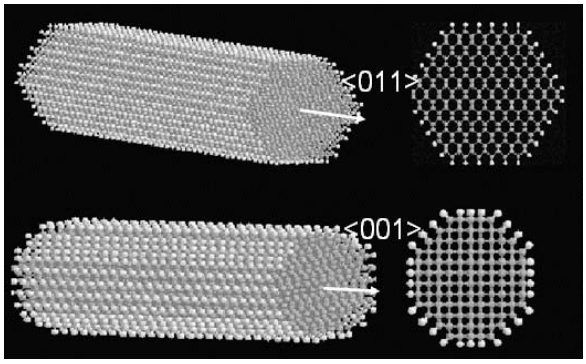

Fig.19. Ball-and-stick illustrations of representative DNRs. Principal axis corresponds to the diamond <011> direction (top),and the diamond <001> direction (bottom) with (011) and (001) facets. Courtesy O. A. Shenderova and D. Brenner.

Stress-strain relations are explicitly macroscopic properties that require a definition of cross-sectional area, therefore (at the nanoscale) a less ambiguous characteristic of strength was found to be the maximum force before fracture for a given structure, rather than the maximum stress. The analysis of fracture force versus diameter for SWNTs, MWNTs, and DNRs was based on forces for bond breaking between individual atoms, and the number of atomic sites in the cross-sectional area of the nanostructures. Shenderova *et al.* [39] examined a zigzag nanotube structure and used the ideal strength value for a graphene sheet from *ab initio* pseudopotential total energy calculations carried out within the local density approximation by Ribeiro *et al.* [53]. The MWNTs were ascribed a fixed inner diameter of 4 nm with various numbers of outer shells, assuming an inter-shell distance of 3.4 Å.

Three orientations for the diamond nanowires were considered with principle axes oriented in [111], [110] or [100] directions. Some representative structures are shown in Fig. 19. The study found that at small diameters, SWNTs are stronger than DNRs because of the superior strength of single bonds in graphene over those in diamond. However, as the diameter increases, the load bearing area increases linearly for SWNTs and as the square of the diameter for nanowires, leading to a larger fracture force for diamond nanowires above a critical diameter of ~1 – 3 nm (depending on the crystallographic orientation of the nanowire axis).

In addition to the fracture force, the strength-to-weight ratio was also considered. To determine the relative strength-to-weight ratios of DNRs and SWNTs, the ratio between the diameter of a nano-rod and a SWNT as a function of nanotube diameter was calculated by the authors for two cases. In each case the condition of equal fracture force and the condition of equal weight of the two structures being compared was ensured. With equal fracture force the weight ratio nano-rod/SWNT was found to be a constant 1.47; however, at diameters smaller than the critical diameter, DNRs were found to require a larger diameter to bear the same load as a related SWNT. With the requirement of equal weight, the ratio of related fracture forces of nanowire/SWNT was found to be 0.68, indicating that at larger diameters nanowires are stronger but at the cost of a lower strength-to-weight ratio.

Similar to the strength analysis above, the stiffness of DNRs and SWNTs was compared by considering them as nanoscale structures. In estimating Young's modulus Y, the authors used the product of Y and $S_{\perp}$ (cross-sectional area per atom), as this product is directly proportional to the nanostructure spring constant. By describing the stress-strain relationship (for uniform tension of a homogeneous system) in terms of Y, $S_{\perp}$ and the resulting deformation e (and making appropriate substitutions), the product of Y and $S_{\perp}$ was calculated as a second derivative of strain energy divided by length attributed to an atom along the direction of the tensile force. This characteristic was found to be significantly higher for graphite than diamond, reflecting that the graphite sp^2 bonds are substantially stiffer than diamond sp^3 bonds, although the bulk materials have comparable stiffness (in-plane for graphite versus any direction in diamond) because of the higher density of diamond, 3.5 g/cm^3 compared to 2.2 g/cm^3 for graphite.

For the situation where the DNRs and SWNTs are under tension, Shenderova *et al.* [39] used a relation for total force-strain. Here a nanostructure stiffness constant was introduced as a coefficient of proportionality between the applied force and elongation, that was dependent on the diameter of the nano-rod (nanotube). By comparing this stiffness constant as a function of diameter, DNRs were found to be stiffer than SWNTs at diameters exceeding ~ 1 nm, thereby making them mechanically viable nanomaterials for structural applications.

3.2. Thermodynamic phase stability

Although all of these models have begun to establish a framework for the structural stability of DNWs and DNRs as a function of morphology and size, these approaches do not directly address the phase

stability 1-D diamond structures. This question was investigated by Barnard and Snook [54], using a thermodynamic model that had previously been devised to examine the phase stability of 0-D nanocarbon [3,4].

The method was based on the heat of formation, as a function of particle size, where the heat of formation of a carbon atom in graphite ($\Delta H_f^0(G)$) and diamond ($\Delta H_f^0(D)$) structures was expressed in terms of the C-C and C-H bond energies E_{CC} and E_{CH}, and dangling bond energy E_{DB}, such that:

$$\frac{\Delta H_f^0(G)}{N_C} = \frac{3}{2}E_{CC}^G + \frac{N_H}{N_C}\left(E_{CH}^G - \frac{1}{2}E_{CC}^G + \Delta H_f^0(H)\right) + \Delta H_f^0(C) + \frac{1}{2}E_{CC}^{vdw}, \quad (7)$$

$$\frac{\Delta H_f^0(D)}{N_C} = 2E_{CC}^D + \frac{N_{DB}}{N_C}\left(E_{DH}^D - \frac{1}{2}E_{CC}^D + \Delta H_f^0(DB)\right) + \Delta H_f^0(C), \quad (8)$$

where, N_C is the number of carbon atoms, N_{DB} is the number of dangling bonds on the surface of the particle and N_H is the number of terminating hydrogen atoms. In these expressions, $\Delta H_f^0(C)$ is the standard heat of formation of carbon at 298.15K, $\Delta H_f^0(H)$ is the standard heat of formation of hydrogen, and E_{CC}^{vdw} is the van der Waals attraction between graphite sheets.

In the case of fullerenic nanocarbon such as fullerenes and SWNTs, as there is no inter-layer attraction $E_{CC}^{vdw}=0$, and the closed shells ensure that N_H/N_C term is also zero, leaving:

$$\frac{\Delta H_f^0(F)}{N_C} = \frac{3}{2}E_{CC}^F + \Delta H_f^0(C). \quad (9)$$

A term for the strain energy (E_{strain}^F) that vanishes in the graphene limit was then added, by first making the assumption that a CNT may be approximated as a homogeneous and isotropic elastic cylinder. This was modelled by considering the bending and stretching of a suitable elastic sheet. The bending energy (E_{bend}) per unit area (A) is given in terms of the sheet thickness (h), by:

$$\frac{E_{strain}}{A} = \frac{\kappa}{2}\int_{-h/2}^{+h/2} dz \frac{z^2}{R^2} = \frac{\kappa h^3}{24R^2}, \quad (10)$$

where κ is the bending modulus of the sheet, and R is the radius of curvature. The strain energy per carbon atom was therefore:

$$\frac{E_{strain}}{N_C} = \frac{A\kappa h^3}{N_C 24R^2}. \quad (11)$$

A cylindrical model was assumed, so that R is equal to the mean radius, $A=2\pi RL$, and $N_C=2\pi RL\rho$. Therefore, an expression for the strain energy per carbon atom was obtained, which was linearly dependent on the inverse square of the curvature of the structure:

$$\frac{E_{strain}}{N_C} = \left(\frac{\kappa h^3}{\rho 24}\right)\frac{1}{R^2} = E_{strain}^F \frac{1}{R^2}. \quad (12)$$

Therefore, the heat of formation for a CNT was given by:

$$\frac{\Delta H_f^0(F)}{N_C} = \frac{3}{2}E_{CC}^F + \Delta H_f^0(C) + \frac{E_{strain}^F}{R^2}. \quad (13)$$

The value of E_{strain}^F was obtained by fitting the calculated energy for all zig-zag and armchair CNTs from n = 3...12 to the inverse of the square of the radius of curvature (see left graph in Fig. 20). The E_{CC}^D and E_{DB}^D for the DNWs was obtained by extrapolating the energy per atom versus the number of dangling surface bonds per atom for the stable dodecahedral, cylindrical and cubic DNW structures described in the last section (see right graph in Fig. 20). The slope and intercept of the linear fit gave values for the cohesive energy of -7.55 eV and a dangling bond energy of 1.32 eV, respectively. These values were used to calculated the atomic heat of formation, which was plotted as a function of the number of carbon atoms per unit length. By extrapolating an empirical best fit Barnard and Snook determined the critical size for the phase transition between DNWs and CNTs to be ~ 450 atoms/nm, as shown in the right graph of Fig. 21. This corresponds to a DNW of ~ 2.7nm in diameter, or a n = 27 armchair nanotube. Below this cross-over CNTs are energetically preferred, whereas over this size DNWs were predicted to be energetically preferred.

However, the heat of formation of DNWs with small diameters were found to vary considerably among the various morphologies, with the dodecahedral nanowires having formation energies similar

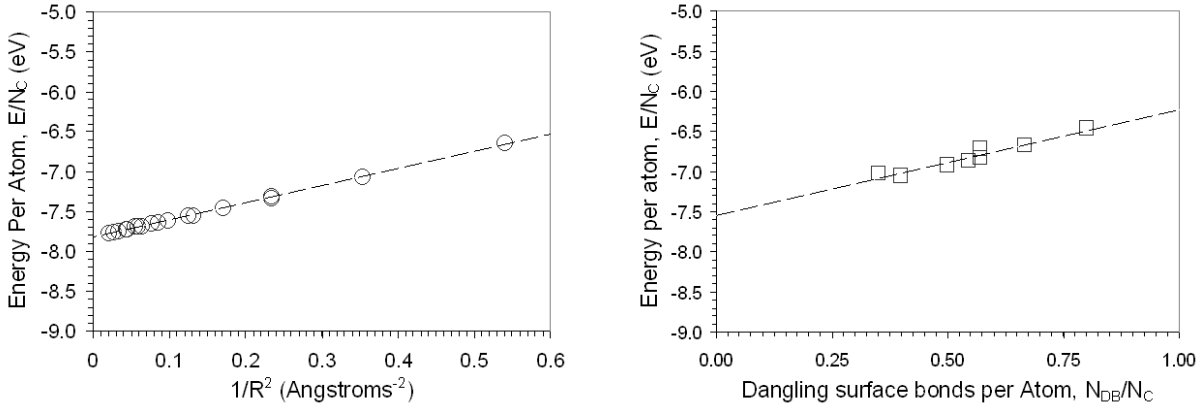

Fig. 20. Energy per atom for the CNTs (left) and stable DNWs (right) plotted as a function of the inverse square of the radius of curvature and the number of dangling bonds per atom, respectively. The linear best fits from which the cohesive energy, strain energy and dangling bonds energies were obtained are also shown. Courtesy A. S. Barnard.

to SWNTs. This significant result indicated that diamond nanowires with C(110) surface facets, and a principle axis in the [100] direction are not only structurally stable, but also almost as energetically favorable as CNTs.

The upper limit of DNW stability was also investigated, using estimates for the heat of formation of graphite made with experimental values for the bond energies [3, 4, 54]. The determination of the cross-over in phase stability between DNWs and graphite required that the number of atoms in the graphite model be appropriately scaled (per unit length), to maintain the dimensional integrity of the system. Two chiral directions, equating to $\theta = 0$ and $\theta = 30°$ (where θ is the chiral angle) were used, and the intersection of the heat of formation as a function of atoms/nm for DNWs with graphite was then obtained for each 'chiral scaling'. The phase stability crossing-point for graphite and DNWs (averaged over morphologies) was found to be 870 and 930 atoms/nm (3.7-3.9 nm in diameter), for $\theta = 0$ and $\theta = 30°$, respectively.

These results indicated a 'window' of stability for DNWs, between approximately 450 to 870-930 atoms/nm (2.7nm to 3.7-3.9 nm in diameter). It is important to not that the upper limit of this range (where graphite becomes energetically preferred) is sensitive to the chiral scaling direction, just as the

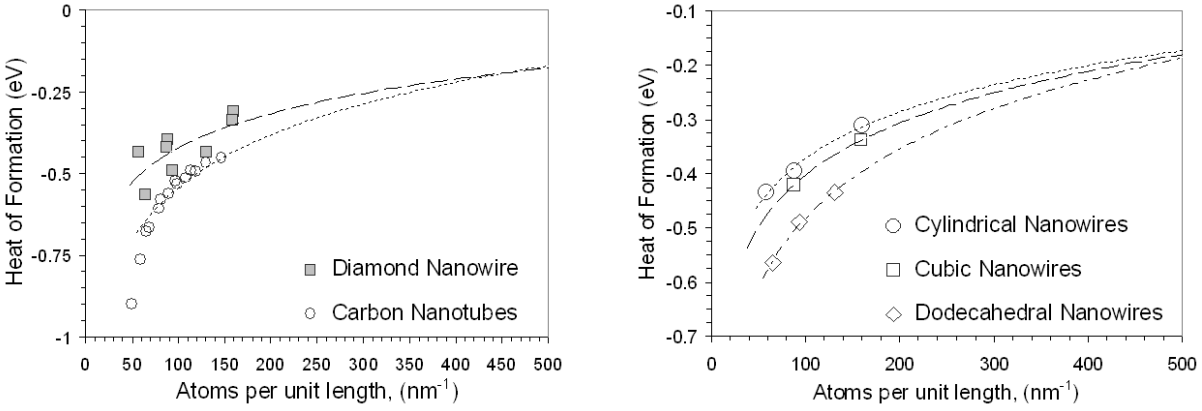

Fig. 21. Comparison of the theoretical heats of formation for stable DNWs and CNTs (left) and comparing the various morphologies of the stable DNWs (right) of Barnard and Snook [55]. The fits are also to guide the eyes. Courtesy A. S. Barnard.

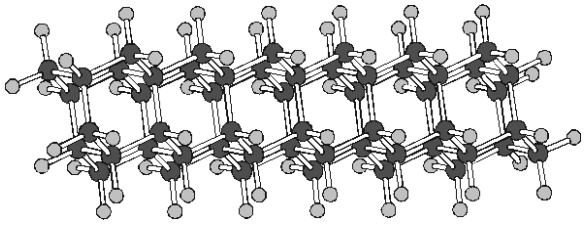

Fig. 22. The small $C_{54}H_{60}$ DNR examined by Zhang *et al.* [13], using quantum mechanical methods. Reprinted from Chemical Physics Letters, Vol.364, R. Q. Zhang, S. T. Lee, C.-K. Law, W.-K. Li and B. K. Teo, Silicon nanotubes: Why not?, p.251, © (2002), with permission from Elsevier.

lower limit of the reported range (where SWNTs become energetically preferred) was sensitive to the DNW morphology [54].

A common theme in the work of Barnard and colleagues outlined earlier in this review is that hydrogenation of DNW surface, promotes structural stability, irrespective of the particulars of the nanowire morphology. Hydrogenated DNWs were not treated by the thermodynamic model described above, leaving the question of how these nanomaterials will compare to CNTs unanswered. This issue has been addressed to briefly by Zhang *et al.* [12], who examined the equilibrium structure of an ultra-fine DNR in direct comparison with a (3,3) CNT, using quantum mechanical methods.

Zhang and colleagues used the PM3 parameterizations [57] of the MNDO semiempirical Hamiltonian [58] throughout their study of the relative stability of representative DNR, CNT, silicon nanowire and silicon nanotube structures. Each structure was geometrically optimized with the PM3 method and at the Hartree-Fock level with the 3-21G and 3-21G(d) basis sets. In the cases of the carbon structures, the DNR and the CNT, the PM3 and HF results were in agreement.

Fig. 22 shows the small $C_{54}H_{60}$ DNR examined in this study. The C-C bonds in this structure were found to be approximately 1.54 Å for the bonds 'perpendicular' to the nano-rod axis and approximately 1.53 Å for the remaining bonds. These lengths are very close to C-C bonds in bulk diamond, and suggest that no contraction of the structure occurred perpendicular principle axis (contraction of the cross-sectional area), whereas a minor contraction occurred in the direction of the principle axis (a contraction of the nanowire length); although this is not discussed in detail by the authors. In the $C_{54}H_{12}$ CNT (a finite CNT fragment with the ends terminated by H atoms), the C-C bond lengths were found to alternate between 1.40 and 1.46 Å (1.38 and 1.45 Å) when relaxed using the PM3 (HF) methods; indicating a certain degree of C=C versus C-C bond localization. The authors attribute the small bond length alternation of about 0.06–0.07 Å to extensive p delocalization in CNTs. Such localization was not observed in the hydrogenated DNR.

Although the energetics of these structure were not presented, the lower degree of variation in the bonds lengths or the DNR (due to the minimization of the energy during the relaxation of the structures) suggests that this structure is reasonably stable, relative to the CNT fragment with the same number of C atoms.

3.3. Experimental progress

To date, structures such as those described in the last section of theoretically modelling of DNWs (above) have not yet been obtained experimentally. Indeed, successes in the fabrication and growth of DNWs and DNRs have been quite limited, and have mainly been in the fabrication of polycrystalline rods of diamond. For example, aligned diamond nanowhiskers have been formed using air plasma etching of polycrystalline diamond films by Baik *et al.* [19, 20], as shown in Fig. 23.

Initially, polycrystalline diamond films of ~4 mm in thickness were grown on a boron-doped silicon (100) wafer (pre-treated by diamond powder to promote nucleation) by use of the hot filament chemical vapor deposition (HFCVD) method. A source of hydrogen gas mixed with 5% methane was thermally activated by tungsten filament heating at 2100 °C and 40 torr. The as-grown diamond films composed of C(100) and C(111) crystalline facets (1x1 cm^2) [21] were then subjected to dry etching under the air plasma generated at 30 mtorr and a radio-frequency (RF) power of 300 mW, with a magnetic field of 60 gauss parallel to the substrate, to which a bias of -470 V was applied. The substrate was not heated, but the temperature rose to 230 °C during etching. The deposition time was varied between 5 and 60 s, with a deposition rate of 0.6 nm/s. Dry etching of the diamond films with molybdenum deposits created well-aligned uniformly dispersed nanowhiskers up to 60 nm in diameter with a density of 50 μm^2. Using this method, the group were able to fabricate high density diamond whiskers with good reproducibility [20]. These diamond nanowhiskers showed well-defined characteristics of diamond [20]. The possible graphitic transformation of the diamond nanowhiskers was also exam-

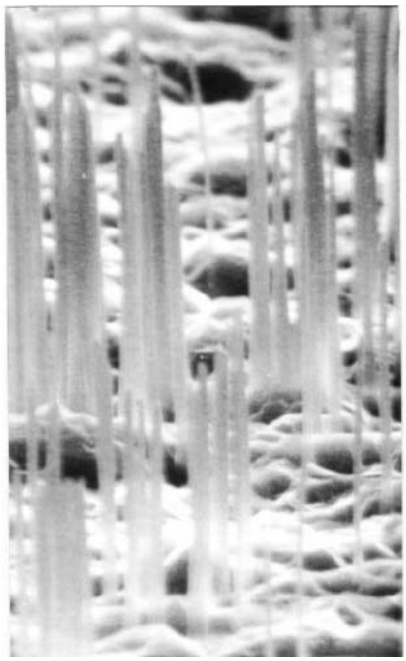

Fig. 23. Magnified SEM micrograph of the 60 nm diamond nanowhiskers (image is 2.5 μm across). Reprinted from Thin Solid Films, Vol.377-378, E.-S. Baik, Y.-J. Baik, S. W. Lee and D. Jeon, Fabrication of diamond nanowhiskers, p.295, © (2000), with permission from Elsevier.

ining by Baik and colleagues using Raman spectroscopy, with results confirming that the surfaces of the whiskers retained the diamond structure during etching [19].

SEM images of the resulting nanostructures are given in Fig. 24, showing the diamond nanowhiskers rising from the remaining diamond film up to approximately 2 μm in height, and with a thickness of 100 nm. The non-random distribution of the nanowhiskers over the film surface can be seen from the top view shown in Fig. 24b, exhibiting a network-like pattern tracing out preferential location of whisker formation. The authors also pointed out that (upon closer inspection) the average size of an individual area enclosed by the nanowhiskers was approximately that of a diamond grain on the etched film surface. This suggested that diamond nanowhiskers may form preferentially at grain boundaries between diamond crystals [19]. The average distance between the whiskers is approximately 60 nm [20].

This aspect of the growth was further investigated using Auger electron spectroscopy, results of which indicated the existence of molybdenum oxides on the tips of the nanowhiskers [20], acting as a mask inhibiting etching of the diamond film underneath. The source of Mo was thought to be the substrate holder, which had sufficient area (about 15 cm in diameter) for direct exposure to the plasma. The authors speculated that upon adsorption, the sputtered Mo atoms would initially form isolated nuclei with sizes ranging from several nanometers to several micrometers. Thus, the formation of the nanowhisker at the grain boundaries was attributed to preferential adsorption of Mo atoms at the grain boundaries. It was also found that the population density of the nanowhiskers decreased as the Mo deposits increased [19]. Although Mo residue could be identified on tip of the nanowhiskers under SEM if large amount of Mo was deposited, the residue

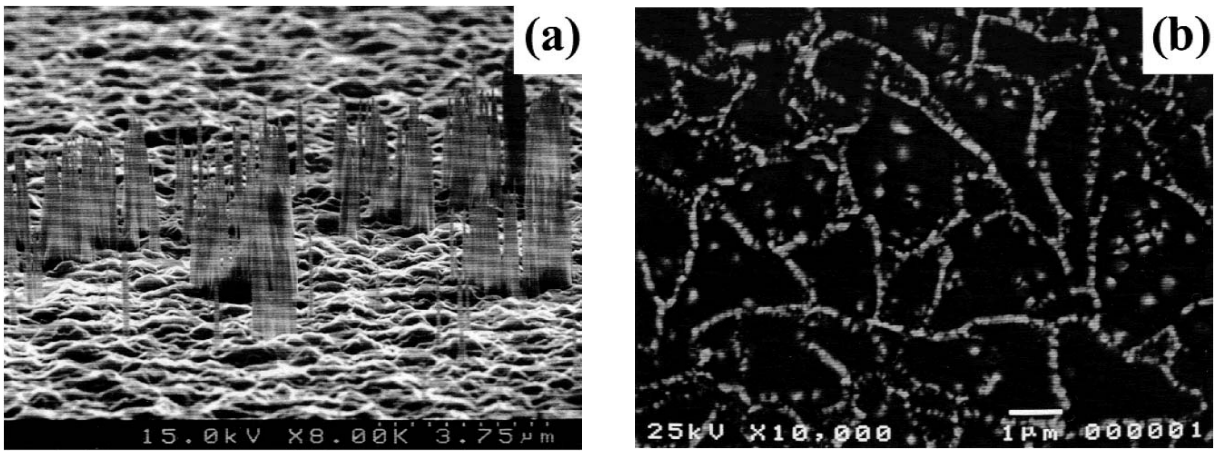

Fig. 24. SEM micrographs of diamond nanowhiskers resulting from etching for 50 minutes aligned perpendicular to the substrate: (a) perspective, and (b) top views. The base plane is diamond. Reprinted from Journal of Materials Research, Vol.15, E.-S. Baik and Y.-J. Baik, Aligned of diamond nanowhiskers}, p.923, © (2000), with permission from MRS.

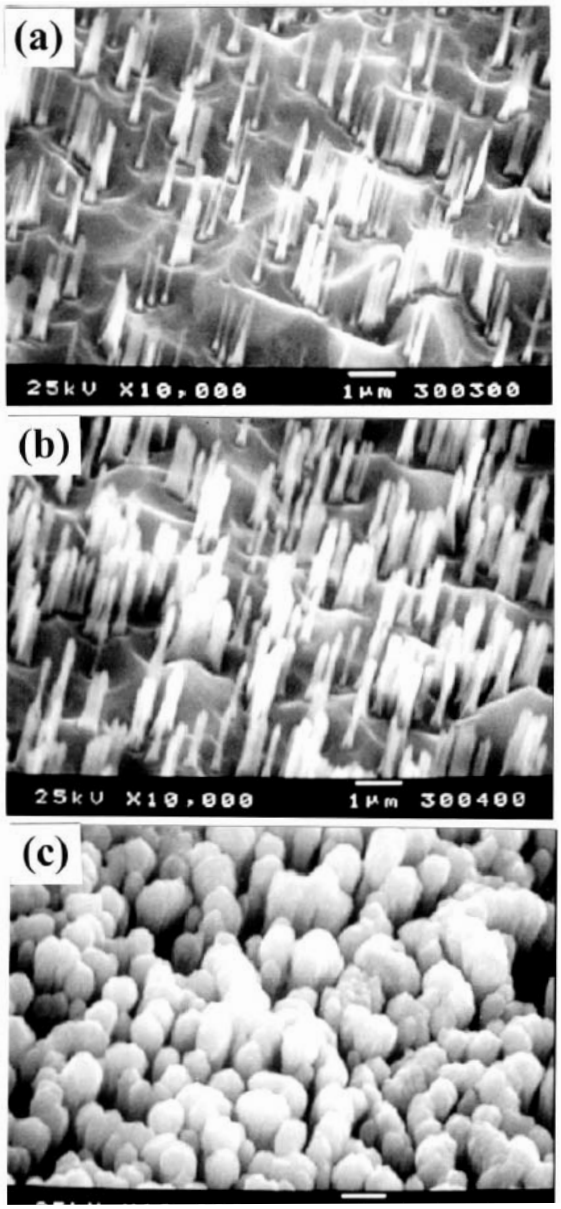

Fig. 25. SEM micrographs of the whiskers formed at different substrate temperatures during the etching. (a) 300, (b) 400 and (c) 500 °C. When the substrate was not heated, the temperature rose to 230C due to the plasma. The nanowhiskers become thicker with increasing temperature because of agglomeration of the Mo clusters. Reprinted from Thin Solid Films, Vol.377-378, E.-S. Baik, Y.-J. Baik, S. W. Lee and D. Jeon, Fabrication of diamond nanowhiskers, p.295, © (2000), with permission from Elsevier.

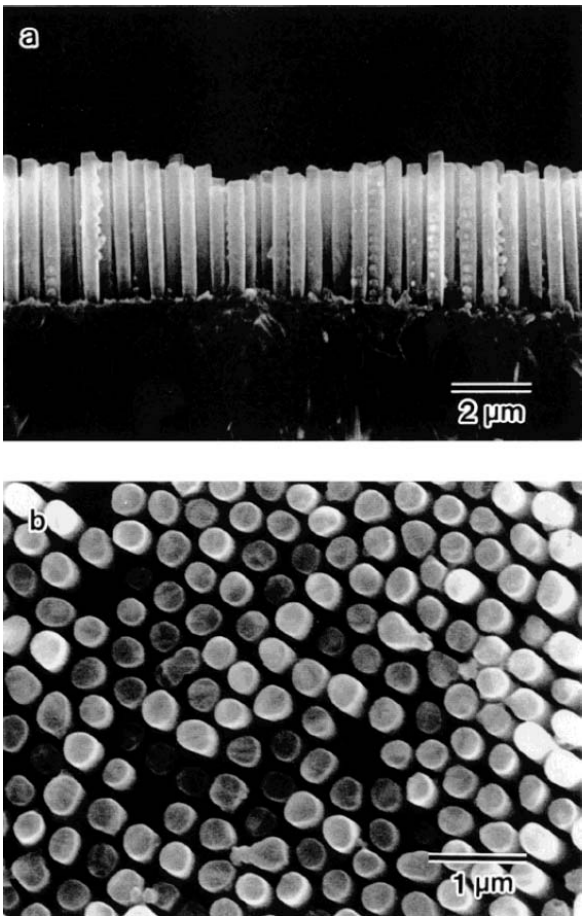

Fig. 26. Scanning electron micrographs of cylindrical structures. (a) Cross-sectional view of the diamond cylinder membrane after dissolving the alumina template. The surface diamond film of the membrane can be seen in the lower part of the image. (b) Top view of the cylinder membrane. Reprinted from Advanced Materials, Vol.13, H. Masuda, T. Yanagishita, K. Yasui, K. Nishio, I. Yagi, T. N. Rao and A. Fujishima, Synthesis of Well-Aligned Diamond Nanocylinders, p.247, © (2001), with permission from Wiley-VCH.

could be removed by rinsing in acid without affecting the nanowhiskers [20].

Baik *et al.* [20] also found that protection of the side of the nanowhiskers had an influence on formation, since the density and morphology of the nanowhiskers appeared to be sensitive to the chamber pressure and the substrate temperature (in addition to the Mo deposition). The nanowhiskers became thicker with increasing substrate temperature (due to the agglomeration of Mo clusters), as shown in Fig. 25, and did not form at all if the chamber pressure was too low or too high.

Polycrystalline diamond nanocylinders with a diameter of approximately 300 nm have also been successfully fabricated, though using different approach. Masuda *et al.* [21] reported the preparation of well-aligned polycrystalline diamond nanocylinders on anodic aluminum oxide templates using

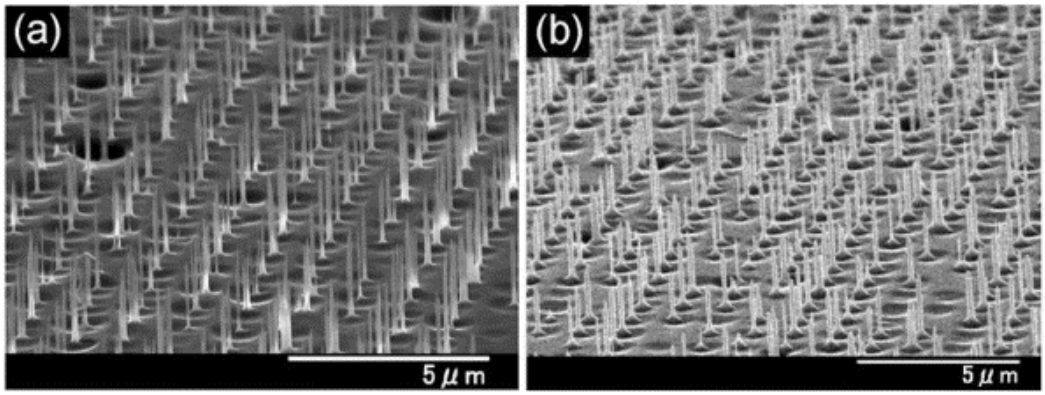

Fig. 27. SEM micrographs of (a) array of diamond whiskers fabricated by RIE and (b) hydrogen plasma treated whiskers, that is, nano-rods of diamond. Reprinted from Diamond and Related Materials, Vol.XX, Y. Ando, Y. Nishibayaski, K. Kobashi and A. Sawabe, 'Nano-rods' of single crystal diamond}, p.XXX, © (2004), with permission from Elsevier.

microwave plasma-assisted CVD and 50 nm nanodiamond particles as seeds. The technique was shown to facilitate the controlled preparation of diamond cylinders with uniform diameter, by varying the template dimensions (see Fig. 26).

The alumina templates were prepared by the authors using electrochemical anodization of aluminum sheet (thickness 0.15 mm) in 0.3 M phosphoric acid at 1 °C under a constant voltage of 190 V for 70 min. The Al metal was etched in a saturated $HgCl_2$ solution when a film thickness of ~ 7 μm was achieved (on the aluminum substrate), followed by etching (in a 10 wt.% phosphoric acid solution) of the bottom part of the oxide film. The resulting well-ordered nanoporous membranes were then used as templates for diamond deposition. The deposition was carried out at a microwave power of 3 kW using hydrogen as a carrier gas, and acetone as the carbon source. The system pressure was kept at 80 torr and the flow rate of the gas mixture was set at 10 sccm. The temperature of the substrate during deposition was estimated to be 1000 °C by optical pyrometer, and the deposition time was 8 hours. This enables the growth of diamond cylinders along the length of the pores.

In this study, straight, vertically aligned, two-dimensional arrays of the diamond nanocylinders with density as high as $4.6 \cdot 10^8$ cylinders/cm^2 were obtained, with the shape of the cylindrical depending upon the size of the nanodiamond seeds. Ordered 300 nm diamond nanocylinder arrays perpendicular to the diamond base with cylinder lengths of about 5 μm are shown in Fig. 26. The nanoarrays were characterized using SEM and Raman spectroscopy. The Raman specta revealed a strong peak at approximately 1334 cm^{-1} (characteristic of diamond) and a broad peak centering at 1440 cm^{-1}, indicating the presence of sp^2 carbon.

The authors concluded by inviting other researchers to adopt the technique and study the physical properties of these arrays for various applications, as the method had proven to be easy to use, had produced highly ordered diamond nanocylinders in high yield, and it was possible to control the dimension of the nanocylinders varying the pore dimensions of the alumina membrane. Still, these structures were composed of polycrystalline material, and are far from the single-crystal 1-D nanostructures examined by theorists.

Most recently, nano-rods of single-crystalline diamond have been reported by Ando *et al.* [22, 23], with high aspect ratios (the height/diameter was approximately 8 for standard array structures and approximately 25 for unique cases). Their proposed microfabrication technique was based on a reactive ion etching (RIE) system, and had also proven useful in the fabrication of single-crystal diamond emitters with very sharp tips (but with the different etching conditions) [59, 60].

In the fabrication of the DNRs, the authors used 300 W RF (13.56 MHz) power and 1.5x2.0x0.3 mm^3 HP-HT synthetic single crystal Ib diamonds substrates with C(100) and C(110) surfaces. Like Baik *et al.* [20,21], etching masks were used; one consisting of oxide impurities acting as micro-masks (sputtered from substrate holder onto the substrate surface during the etching process), and another consisting of arrays of Al dots (~ 1.0 μm) diameter

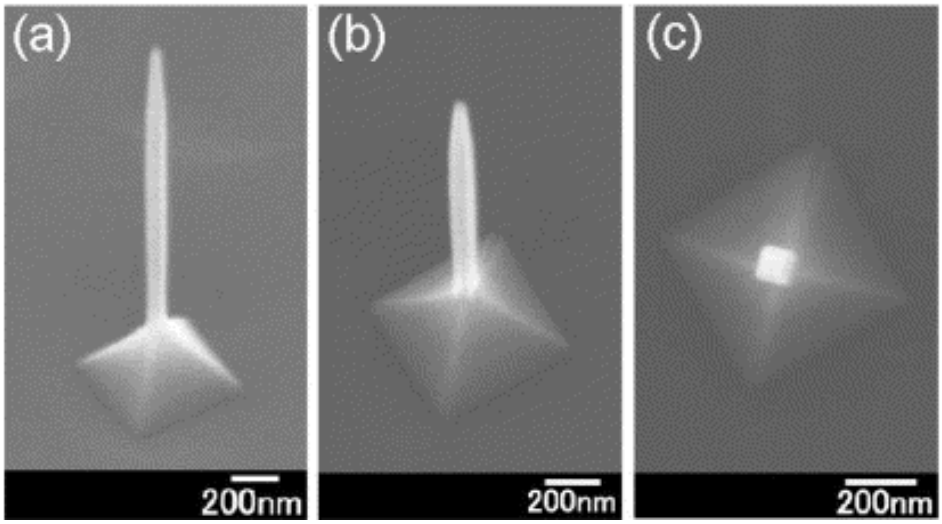

Fig. 28. Nano-rod fabricated on HP-HT synthetic diamond with (100) surface observed by SEM with different angles: (a) 458 (b) 708 (c) 908 (top view). Reprinted from Diamond and Related Materials, Vol.XX, Y. Ando, Y. Nishibayaski, K. Kobashi and A. Sawabe, 'Nano-rods' of single crystal diamond, p.XXX © (2004), with permission from Elsevier.

and ~0.5 μm thickness) formed by a conventional photolithography. The etched diamond was treated in HF acid after RIE in order to remove non-diamond components, followed by microwave plasma post-treatment. Although the substrate holder was water cooled, the diamond temperature was found to increased to 470 – 570K during the experiments.

The authors used a field emission type scanning electron microscopy (FE-SEM) to observe the morphology and size of the resulting DNRs, as shown in Fig. 27. Fig. 27 illustrating the results of a reactively ion etched surface of diamond Ib (100) substrate patterned with Al dots. Detailed information about the fabrication method of the diamond whiskers was discussed in reference [59], however, the random alignment of the nano-rods was attributed to oxide impurities sputtered from the substrate holder during the etching were used as micro-masks for this experiment [59, 60].

The growth (or etching) rate of homoepitaxially grown diamond on the DNR surface was however investigated, as a function of the gas pressure. The growth rate of 7-180 nm/h at 3.3 kPa was found to decrease with increase of the gas pressure, although etching of some DNRs was observed at 4.7 and 5.3 kPa. In general, the shape of the DNR (due to the dependence of the growth on direction) was found to change as a function of the treatment time in hydrogen plasma. The results indicates that the growth rate for the <110> direction was larger than for the <100> direction in the initial stages of growth, resulting in a thin DNR with a rectangular parallelepiped cross-section (see Fig. 28). Note that the growth of the pyramidal shape of diamond at the base of the DNR in Fig. 28 was found to be due to a larger growth rate at a reentrant corner, and the whisker-like tip is terminated by a tiny (100) facet. After a thin rod was formed, the growth in the <100> direction increases, so that the rectangular cross-section persists as the diameter of the nano-rod increases.

Using these results, the Ando and colleagues were able to create arrays of the DNRs, 50-200 nm in diameter and several microns in height, as shown in Fig. 29. Figs. 29a and 29b show the nano-rods parallel to <100> and <111> direction fabricated on the tilted (110) surface of diamond, respectively. It is important to note here that the <100> direction has predominated over the <110> direction, as predicted by the theoretical studies outlined in the previous section, even on a tilted (110) surface. The DNRs grow at an angle to the surface to accommodate this growth direction. It is not clear from Fig. 29 whether the <111> DNRs have also growth at an angle with respect to the substrate, an no rigorous investigation of this growth direction has been undertaken with a high level of theory. Still, Ando *et al*. [23] have shown that since these single-crystal DNRs have the crystal facets, their morphology may

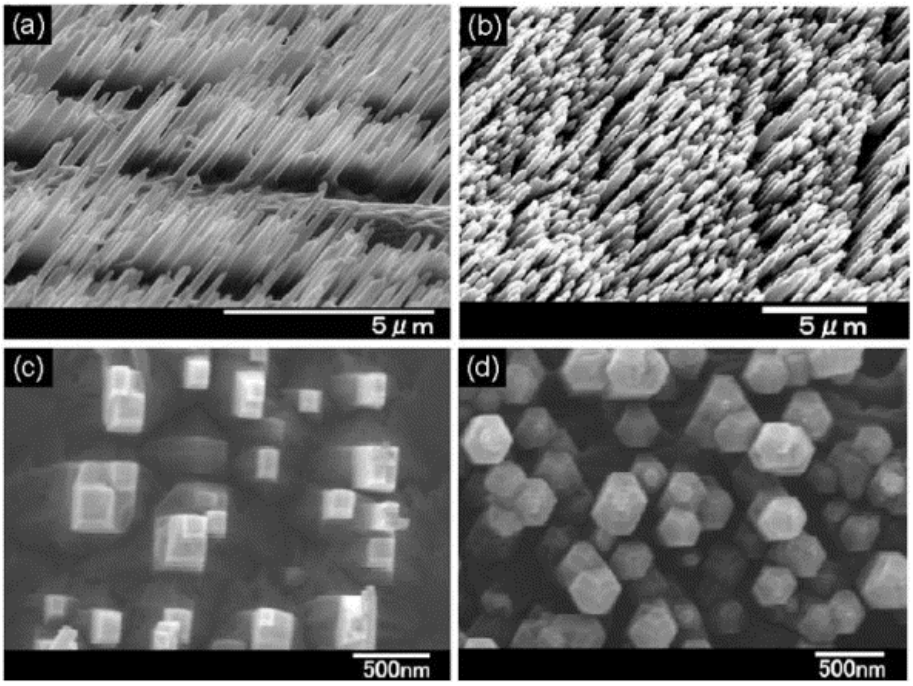

Fig. 29. Nano-rods parallel to (a) <100> and (b) <111> direction fabricated on tilted (110) surface of diamond. (c) and (d) show the top view of the rods in (a) and (b), respectively. Reprinted from Diamond and Related Materials, Vol. XX, Y. Ando, Y. Nishibayaski, K. Kobashi and A. Sawabe, 'Nano-rods' of single crystal diamond, p.XXX, © (2004), with permission from Elsevier.

be controlled by changing the crystal orientation of diamond substrate.

4. FUTURE DIRECTIONS

Although the successful synthesis has been limited, and subsequent production of DNWs and DNRs in has not yet been realized, the current research does suggest that a future exists for these nanostructures. The work of theorists have indicated that while certain morphological criteria are required to achieve structural [35-37, 43] and thermodynamic stability [54], suitable 1-D nanocarbon structures may be expected to withstand reasonable temperatures [38]. The work of experimentalists have shown that a number of possible synthesis routes exist [19-23], depending upon the type of structures required, and that the shape and orientation of these diamond nanomaterials maybe controlled [20, 23]. Once produced, it has been predicted that DNWs and DNRs may have exceptional mechanical [39] and electronic properties [61], as well as their use in structural applications [17], making them a potentially useful commodity.

Still, a great deal of work has yet to be done. It is still not possible to tailor these structures to the precise needs of nanotechnologists, and the present structures are not yet suitable for use in most nanodevices. Experimental characterization of the electronic and optoelectronic properties of the various nanowhiskers and nano-rods have not yet been reported, nor has the structural stability of these structures been examined under irradiation or annealing. In addition to this, the role of defects and impurities in the structure and stability of 1-D diamond nanostructures is not yet understood. Some preliminary theoretical studies have been undertaken using ab initio methods by Barnard *et al*. [62] to examine the effect of various dopants on the stability of ultra-fine cylindrical DNWs. These studies examined the effects of boron, nitrogen, oxygen, aluminum, phosphorus and sulphur included equidistant along the axis of the nanowire (showing that boron and phosphorus dopants are structurally preferred), but a more rigorous investigation is required to examine the effects of dopants at the center and at the surface of larger nanowires.

In general, this area of research is still in it's infancy but shows great promise for the future.

ACKNOWLEDGMENTS

This work was supported in part by the U.S. Department of Energy's Office of Basic Energy Sciences, Division of Materials Science, under contract no. W-31-109-ENG-38. I would also like to greatly acknowledge Ş. Erkoç, S.T. Lee, R.Q. Zhang, M. Menon, Y.-J Baik, Y. Ando, O.A. Shenderova and D. Brenner for providing figure images; the Victorian Partnership for Advanced Computing and the Australian Partnership for Advanced Computing supercomputer center for their supporting of this project; and Larry A. Curtiss for assistance in preparing this review.

REFERENCES

[1] Y. Gogotsi // *Cryst. Growth Design* **1** (2001) 179.
[2] O. A. Shenderova, V. V. Zhirnov and D. W. Brenner // *Crit. Rev. Sol. State and Mater. Sci* **27** (2002) 227.
[3] A. S. Barnard, S. P. Russo and I. K. Snook // *J. Chem. Phys.* **118** (2003) 5094.
[4] A. S. Barnard, S. P. Russo and I. K. Snook // *Phys. Rev. B* **68** (2003) 73406.
[5] S. Iijima // *Nature* **354** (1991) 56.
[6] P. J. F. Harris, *Carbon Nanotubes and Related Structures* (Cambridge University Press, Cambridge, UK (1999).
[7] P. Yang, Y. Wu and R. Fan // *Int. J. Nanosci.* **1** (2002) 1.
[8] Y. F. Zhang, L. S. Liao, W. H. Chan and S. T. Lee // *Phys. Rev. B* **61** (2000) 8298.
[9] Z. Zhang, X. H. Fan, L. Xu, C. S. Lee and S. T. Lee // *Chem. Phys. Lett.* **337** (2001) 18.
[10] W. Shi, Y. Zheng, H. Peng, N. Wang, C. S. Lee and S. T. Lee // *J. Am. Ceram. Soc.* **83** (2000) 3228.
[11] Z. Pan, H. L. Lai, F. C. K. Au, X. Duan, W. Zhou, W. Shi, N. Wang, C. S. Lee, N. B. Wong, S. T. Lee and S. Xie // *Adv. Mater.* **12** (2000) 1187.
[12] R. Q. Zhang, S. T. Lee, C.-K. Law, W.-K. Li and B. K. Teo // *Chem. Phys. Lett.* **364** (2002) 251.
[13] Y. H. Tang, N. Wang, Y. F. Zhang, C. S. Lee, I. Bello and S. T. Lee // *Appl. Phys. Lett.* **75** (1999) 2921.
[14] R.-M. Liu, J.-M. Ting, J.-C. A. Huang and C.-P.Liu // *Thin Solid Films* **420** (2002) 1450.
[15] S. Botti, R. Ciardi, M. L. Terranova, S. Piccirillo, V. Sessa and M. Rossi // *Chem. Phys. Lett.* **355** (2002) 395.
[16] A. Xia, Z. Huizhao, Y. Li and X. Chengshan // *Appl. Surf. Sci.* **193** (2002) 87.
[17] K. E. Drexler, *Nanosystems: Molecular, Machinery, Manufacturing and Computation* (Wiley, New York ,1992).
[18] B. V. Derjaguin, D. V. Fedoseev, V. M. Lukyanovich, B. V. Spitsyn, V. A. Ryabov and A. V. Lavrentyev // *J. Cryst. Growth* **2** (1968) 380.
[19] E.-S. Baik, Y.-J. Baik and D. Jeon // *J. Mater. Res* **15** (2000) 923.
[20] E.-S. Baik, Y.-J. Baik, S. W. Lee and D. Jeon // *Thin Solid Films* **377** (2000) 295.
[21] H. Masuda, T. Yanagishita, K. Yasui, K. Nishio, I. Yagi, T. N. Rao and A. Fujishima // *Adv. Mat.* **13** (2001) 247.
[22] Y. Ando, Y. Nishibayaski, K. Kobashi and A. Sawabe, In: Proc. of European Conference on Diamond, Diamond-like Matierals, Carbon Nanotubes, Nitrides and Silicon Carbide: Mechanical and Thermal Applications (Salzburg, Austria, 2003).
[23] Y. Ando, Y. Nishibayaski, K. Kobashi and A. Sawabe // *Diamond and Relat. Mater.* (2004), in press.
[24] V. L. Kuznetsov, A. L. Chuvilin, Y. V. Butenko, I. Y. Mal'kov and V. M. Titov // *Chem. Phys. Lett.* **209** (1994) 72.
[25] S. Tomita, T. Sakurai, H. Ohta, M. Fujii and S. Hayashi // *J. Chem. Phys.* **114** (2001) 7477.
[26] F. Banhart and P.M. Ajayan // *Nature* **382** (1996) 433.
[27] M. Zaiser and F. Banhart // *Phys. Rev. Lett.* **79** (1997) 3680.
[28] M. Zaiser, Y. Lyutovich and F. Banhart // *Phys. Rev. B* **62** (2000) 3058.
[29] N. W. Winter and F. H. Ree // *Jounal of Computer-Aided Materials Design* **5** (1998) 279.
[30] V. L. Kuznetsov, I. L. Zilberberg, Y. V. Butenko, A. L. Chuvilin and B. Seagall // *J. Appl. Phys.* **86** (1999) 863.
[31] F. Fugaciu, H. Hermann and G. Seifert // *Phys. Rev. B* **60** (1999) 10711.
[32] A. S. Barnard, S. P. Russo and I. K. Snook // *Phil. Mag. Lett.* **83** (2003) 39; *Int. J. Mod. Phys. B* **17** (2003) 3865; *Diamond and Relat. Mater.* **12** (2003) 1867.

[33] J. Y. Raty, G. Galli, C. Bostedt, T. W. Buuren and L. J. Terminello // *Phys. Rev. Lett.* **90** (2003) 37402.
[34] A. S. Barnard, S. P. Russo and I. K. Snook // *J. Nanosci. Nanotech* **4** (2004) 142.
[35] A. S. Barnard, S. P. Russo and I. K. Snook // *Nano Lett.* **3** (2003) 1323.
[36] A. S. Barnard, S. P. Russo and I. K. Snook // *Surf. Sci.* **538** (2003) 204.
[37] A. S. Barnard, S. P. Russo and I. K. Snook // *Phil Mag.* (2004), in press.
[38] O. B. Malcioğlu and Ş. Erkoç // *Int. J. Mod Phys. C* **14** (2003) 441.
[39] O. A. Shenderova, D. W. Brenner and R. S. Ruoff // *Nano Lett.* **3** (2003) 805.
[40] Ş. Erkoç // *Int. J. Mod Phys. C* **11** (2000) 1247.
[41] J. Tersoff // *Phys. Rev. Lett.* **61** (1988) 2879.
[42] Ş. Erkoç and O. B. Malcioğlu // *Int. J. Mod Phys. C* **13** (2002) 367.
[43] M. Menon, E. Richter, P. Raghavan and K. Teranishi // *Superlattices and Microsctructures* **27** (2000) 577.
[44] M. Menon, E. Richter and R. Subbaswamy // *J. Chem. Phys.* **104** (1996) 5878.
[45] G. Kresse and J. Hafner // *Phys. Rev. B* **47** (1993) RC558.
[46] G. Kresse and J. Hafner // *Phys. Rev. B* **54** (1996) 11169.
[47] D. Vanderbilt // *Phys. Rev. B* **41** (1990) 7892.
[48] G. Kresse and J. Hafner // *J. Phys.:Condens. Matter.* **6** (1994) 8245.
[49] J. Perdew and Y. Wang // *Phys. Rev. B* **45** (1992) 13244.
[50] A. S. Barnard, *Ab initio Modelling of Nanocrystalline Diamond in 0 and 1 Dimensions* (Ph.D Thesis, RMIT University, Melbourne, VIC, AUST, 2003).
[51] X. Zhao, Y. Ando, Y. Li, M. Jinno and T. Suzuki // Phys. Rev. Lett. **90** (2003) 187401.
[52] Y. Guo, Ph.D., Thesis (California Institute of Technology, 1992).
[53] F. J. Riberio, D. J. Roudy and M. L. Cohen // *Phys. Rev. B* **65** (2002) 153401.
[54] A. S. Barnard and I. K. Snook // *J. Chem. Phys.* (2004), in press.
[55] X. Hua, T. Çağin, J. Che and W. A. Goddard III // *Nanotechnology* **11** (2000) 85.
[56] *Handbook of Chemistry and Physics, 81st Edition* (CRC Inc., Boca Raton, 2000 - 2001).
[57] J. J. P. Stewart // *J. Comput. Chem.* **2** (1989) 209.
[58] M. J. S. Dewar and W. J. Thiel // *J. Am. Chem. Soc.* **99** (1977) 4899.
[59] Y. Ando, Y. Nishibayashi, H. Furuta, K. Kobashi, T. Hirao and K. Oura // *New Diamond Front. Carbon Technol.* **12** (2002) 137.
[60] Y. Nishibayashi, Y. Ando, H. Furuta, K. Kobashi, H. Furuta, K. Meguro, *et al.* // *Mol. Cryst. Liq. Cryst.* **386** (2002) 183.
[61] A. S. Barnard, S. P. Russo and I. K. Snook // *Phys. Rev. B* **68** (2003) 235407.
[62] A. S. Barnard, S. P. Russo and I. K. Snook // *Phil. Mag.* **83** (2003) 2301; *Phil.Mag.* **83** (2003) 2311.